February 24, 1975

To the Graduate Council:

I am submitting herewith a thesis written by Gordon Ming Sze entitled "The Interaction of Melt Spinning, Drawing, Twisting, Heat Setting and Untwisting on the Crystalline Morphology and Mechanical Properties of Polyethylene Fibers." I recommend that it be accepted in partial fulfillment of the requirements for the degree of Master of Science, with a major in Chemical Engineering.

J. E. Spruiell

Joseph E. Spruiell, Major Professor

We have read this thesis and recommend its acceptance:

Edward S. Clark

James L. White

Accepted for the Council:

Hilton A. Smith

Vice Chancellor
Graduate Studies and Research

THE INTERACTION OF MELT SPINNING, DRAWING, TWISTING, HEAT SETTING AND UNTWISTING ON THE CRYSTALLINE MORPHOLOGY AND MECHANICAL PROPERTIES OF POLYETHYLENE FIBERS

A Thesis

Presented for the

Master of Science

Degree

The University of Tennessee

Gordon Ming Sze

March 1975

ACKNOWLEDGEMENTS

The author wishes to express his deepest and sincere appreciation to both Professor J. E. Spruiell and Professor J. L.White for their advice, guidance and patience through this research. Acknowledgement is made to Mr. B. L. McGill, Ms. E. K. Leonard and the entire Chemical and Metallurgical faculty and staff for their cooperation and assistance.

Sincere appreciation is also expressed to Dr. C. J. Noel for allowing me to use the fiber twisting equipment belonging to the Department of Textiles, College of Home Economics.

Finally, thanks are extended to the National Science Foundation and to Professor H. F. Johnson, Head of the Department of Chemical and Metallurgical Engineering, for the financial aid which was provided.

1197720

ABSTRACT

The purpose of this investigation was to examine the effects of a series of sequential deformation and thermal treatments on the crystalline morphology and mechanical properties of melt spun high density polyethylene. The polymer studied was Phillips Marlex EMB 6050 with a melt index of 5.0. The treatments included twisting of spun filaments, drawing, twisting of drawn fibers, heat setting at 120°C, and untwisting of twisted and heat set fibers. At each treatment step the fiber structure was investigated by scanning electron microscopy, wide angle x-ray diffraction and small angle x-ray diffraction. The mechanical properties were characterized by performing tensile tests.

Drawing results in very high crystalline orientation, fibrillation and large increases in modulus and tensile strength. The natural draw ratio and total draw ratio for the spun filament depend on the orientation developed in the melt spinning process. At a draw ratio slightly greater than the natural draw ratio the amount of fibrillation depends on the spinning condition.

Twisting of either as-spun or drawn fibers decreased the axial orientation, modulus, tensile strength, and usually also the elongation to break of the fibers. The changes in these properties increased with twist angle. Twisting also caused a transformation of a small part of the polyethylene sample to the monoclinic crystal modification. As-spun filaments exhibit necking and yield point behavior. Twisting gradually removes the yield point and causes a more uniform elongation

when the filaments are loaded in tension.

To a good first approximation, the change in orientation and modulus of drawn fibers with twist angle could be predicted using a model originally meant to describe the mechanics of yarns. It was assumed that the fibrils in the drawn and twisted fiber are analogous to the fibers of a twisted yarn.

Heat setting caused healing of voids generated during drawing and increased the perfection and periodicity of the stacking of lamellar crystals. Heat setting also caused the monoclinic polyethylene to transform back to the orthorhombic form, and it increased the modulus and tensile strength.

Untwisting returned the orientation in the fiber to essentially that which it would have if it had not been twisted. However, scanning electron microscopy examination showed that the fibrils were not simply returned to their untwisted form, but that they contained numerous kink bands.

TABLE OF CONTENTS

CHAPTER		PAGE
I.	INTRODUCTION	1
II.	BACKGROUND AND LITERATURE SURVEY	4
	Supermolecular Structure of Semicrystalline Polymers	4
	Plastic Deformation of Semicrystalline Polymers	6
	False-Twisting Texturing Process	18
III.	EXPERIMENTAL DETAILS	22
	Material	22
	Cold-Drawing	22
	Fiber Twisting	22
	Fiber Heat Setting	24
	Scanning Electron Microscopy (SEM)	24
	X-Ray Diffraction Studies	27
	Mechanical Property Measurements	29
IV.	RESULTS AND DISCUSSION	32
	As-Spun and Twisted Spun Fibers	32
	Drawn Fibers	41
	Drawn Twisted Fibers	51
	Twisted Drawn Fibers	55
	Heat Setting of Twisted Fibers	66
	Untwisted Fibers	69
V.	CONCLUSIONS AND RECOMMENDATIONS	83
LIST OF REFERENCES		86

CHAPTER PAGE

APPENDIX 91

VITA 96

LIST OF FIGURES

FIGURE		PAGE
1.	Diagram Illustrating the Proposed Fringed Micelle Structure of Semicrystalline Polymers.	5
2.	Diagrammatic Representation of a Portion of a Lamellae Crystallite with the Polymer Chains in a Regularly Folded Array	7
3.	Peterlin's Model of Transformation from a Spherulitic into a Fibrillar Structure	12
4.	Schematic of X-Ray Diffraction Patterns Showing 2θ and χ . .	16
5.	The C-Axis Tilt Angle ϕ and ϕ_m on the Annuli of Radius r and R.	17
6.	Tilt Angle ϕ and Angle β of a Crystallographic Plane in a Fiber	19
7.	A Schematic Diagram of False-Twist Texturing Principle and Process.	20
8.	Twist Tester	23
9.	Illustration of Fiber Peeling Technique.	25
10.	Specimen Holder for Scanning Electron Microscopy	26
11.	Method of Mounting a Fiber on the Specimen Holder.	28
12.	Fiber Frame.	30
13.	Loading the Twisted Fiber on the Frame to the Instron Grips.	31
14.	X-Ray Patterns of HDPE (MI = 5.0) PE01 (100 m/min)	33

FIGURE PAGE

15. X-Ray Patterns of HDPE (MI = 5.0) PE07 (556 m/min). 36

16. Scanning Electron Micrographs of HDPE Fibers. 38

17. PE01 (100 m/min) Force Versus Percent Elongation at Room Temperature, Twist at Various Degree. 39

18. PE07 (556 m/min) Force Versus Percent Elongation at Room Temperature, Twist at Various Degree. 40

19. Diffraction Patterns of HDPE (PE01) Fibers and Its Scanning Electron Micrograph. 43

20. Diffraction Patterns of HDPE (PE07) Fibers and Its Scanning Electron Micrograph. 46

21. Scanning Electron Micrographs of "Peeled" HDPE Fibers . . . 47

22. Stress Versus Percent Elongation Curve of HDPE (MI = 5.0). 50

23. X-Ray Patterns of HDPE (MI = 5.0) PE01 (100 m/min). 52

24. X-Ray Patterns of HDPE (MI = 5.0) PE07 (556 m/min). 53

25. Scanning Electron Micrographs of Drawn Twisted Fibers . . . 54

26. Diffraction Patterns of HDPE (PE01) Fibers (D.R. 10). . . . 56

27. Diffraction Patterns of HDPE (PE07) Fibers (D.R. 4) 57

28. Scanning Electron Micrograph of HDPE Fibers PE01, D.R. 10, Twist 100 Turns/Inch 60

29. Stress Versus Strain Curve of Drawn PE01 (100 m/min) with Draw Ratio 10, Twist at Various Amounts at Room Temperature 61

30. Stress Versus Strain Curve of Drawn PE07 (556 m/min) with

FIGURE PAGE

Draw Ratio 4, Twist at Various Amounts at Room Temperature 62

31. Effect of Twist Angle on Relative Breaking Load of Drawn HDPE Fibers (PE01 and PE07) at Room Temperature . . 63

32. Effect of Twist Angle on Relative Modulus of Drawn HDPE Fibers (PE01 and PE07) at Room Temperature. 65

33. Diffraction Patterns of HDPE (PE01) Fibers (D.R. 10). . . . 67

34. Diffraction Patterns of HDPE (PE07) Fibers (D.R. 4) 68

35. Stress Versus Strain Curve of Drawn PE01 (100 m/min) with Draw Ratio 10, Twist Various Amounts at Room Temperature, Heat Set at 120°C for 30 Minutes. 70

36. Stress Versus Strain Curve of Drawn PE07 (556 m/min) with Draw Ratio 4, Twist Various Amounts at Room Temperature, Heat Set at 120°C for 30 Minutes. 71

37. Effect of Twist Angle on Relative Breaking Load of Drawn HDPE Fibers (PE01 and PE07) at 120°C. 72

38. Effect of Twist Angle on Relative Modulus of Drawn HDPE Fibers (PE01 and PE07) at 120°C 73

39. Diffraction Patterns of HDPE (PE01) D.R. 10 74

40. Diffraction Patterns of HDPE (PE07) D.R. 4. 75

41. WAXS and SAXS Patterns of HDPE. 77

42. Scanning Electron Micrograph of PE01 with Draw Ratio of Ten, Twist at 100 Turns/Inch and Untwist 79

43. Scanning Electron Micrographs of PE03 (50 m/min), Etched

FIGURE PAGE

in Fuming Nitric Acid for One Hour, D.R. 10, Twisted 125 Turns/Inch, Untwisted 80

44. Stress Versus Strain Curve of Draw PE01 Fiber (100 m/min) with Draw Ratio 10, Twist at Various Amount, Heat Set at 120°C for 30 Minutes, Then Untwisted Back to Initial State 81

45. Stress Versus Strain Curve of Drawn PE07 Fiber (556 m/min) with Draw Ratio 4, Twist at Various Amounts at Room Temperature, Heat Set at 120°C for 30 Minutes, Untwisted Back to Initial State 82

CHAPTER I

INTRODUCTION

At one time, the major fibers in the textile world were cotton, silk and wool. In 1880, a French chemist, the Count de Chardonnet (64) developed a process by which man-made fibers could be produced from nitrated cellulose. By the mid 1920's, the American man-made fiber industry was well organized. In 1932, Carothers and Hill (8) of DuPont were the first to make a wholly synthetic fiber by spinning fibers from both melt and from solution (dry spinning). Since those days, the development of new fibers has proceeded at a remarkable rate and there are now on the market many materials of widely differing chemical constitutions, such as polypropylene, polyester, nylon 66, and nylon 6. The outlook for continued growth of the market is extremely rosy.

The properties of any polymer depend to some extent on the chemical structure and the arrangement of the units, both on a molecular and a supermolecular level that go to make up the material. Synthetic fiber producers have made a major effort to develop techniques to improve the mechanical properties of synthetic fibers. The fibers are generally drawn, i.e., permanently stretched out in the solid state to produce highly oriented structures with much higher modulus and strength than the spun fibers. Because of the importance of this basic process, it has received and continues to receive much attention in the fiber research literature. A second development has been the production of bulked and stretchy yarns which show apparent greater volume and high

level of stretch and recovery (4, 62). Many methods have been devised to produce such texturized yarns. They include (1) false-twisting, (2) stuffer-box crimping, (3) edge crimping, (4) gear crimping, and (5) steam jet bulking. Of these, the false-twisting (twist-heat-set-untwist) process is by far the most important. Unfortunately, little seems to be known of the structure of twisted and forcibly untwisted fibers, especially under the temperature conditions involved in industrial false-twisting processes. As is quite obvious, the properties of fibers are reflections of their structures; a great deal of scientific effort has already been expended in establishing relationships between fiber structures and properties and in modifying structure to achieve a desirable product. The present research represents a further extension of this previous work to establish the structure and properties of drawn, twisted and forcibly untwisted polyethylene fiber.

The purpose for choosing polyethylene fiber is twofold. First, in recent years, the Department of Chemical and Metallurgical Engineering has developed a research program on fiber processing. The early work emphasized rheological and heat transfer phenomena in the spinline (2, 9). In turning to structure development in spinning and drawing, Abbott and White (1) chose polyethylene with its orthorhombic unit cell as a starting point and determined its crystallinity and orientation factors for the three crystallographic axes as a function of spinning conditions. Dees and Spruiell (12) determined the variation in level of crystallinity, crystallization kinetics and orientation factors in polyethylene with position along the spinline. In a later study, White, Dharod and Clark (61) investigated the interrelationship between the

melt spinning and drawing variables on the nature of the crystallinity and molecular orientation and also their influence on the mechanical properties. The present work is a continuation of this previous fiber processing research. Secondly, polyethylene has the simplest crystal structure found in common polymers. The morphology of crystallization also is better known than that of the other polymers. Though polyethylene fiber has little commercial merit, it provides a useful model system to study the structural changes which accompany texturing.

The research in this thesis has been performed with high density (linear) polyethylene fiber which was prepared by J. R. Dees (13) in his Ph.D. dissertation.

CHAPTER II

BACKGROUND AND LITERATURE SURVEY

A. SUPERMOLECULAR STRUCTURE OF SEMICRYSTALLINE POLYMER

Pioneering studies of the structure and properties of natural cellulosic fibers, beginning in the middle of the 19th century, form the basis of many polymer concepts which are still widely held today. In the late 1920's, Mark and Meyer (32) proposed the micellar theory. It assumed that there was crystalline structure within the micelle which was supposed to be the smallest structure aggregate of macromolecules. The discovery that fibers and other plant materials were able to diffract x-rays provided great support for the micelle theory. At this time, a completely different view was taken by Staudinger (58), following his deductions from measurements of the viscosities of polymer solutions that the molecules were much longer. He suggested that a polymer was a large continuous imperfect crystal, with the crystalline imperfections being associated with the ends of the molecular chains. An amorphous polymer, according to the continuous structure concept, consisted of a random network of intertwined polymer molecules with no structure regularity. In 1930, Hermann, Gergross and Abitz (26) modified the previous concepts and proposed fringed micelles. A schematic illustration of the fringed micelle model is shown in Figure 1. In this model, crystalline micelles were considered to be embedded in amorphous regions, however, individual polymer chains were able to

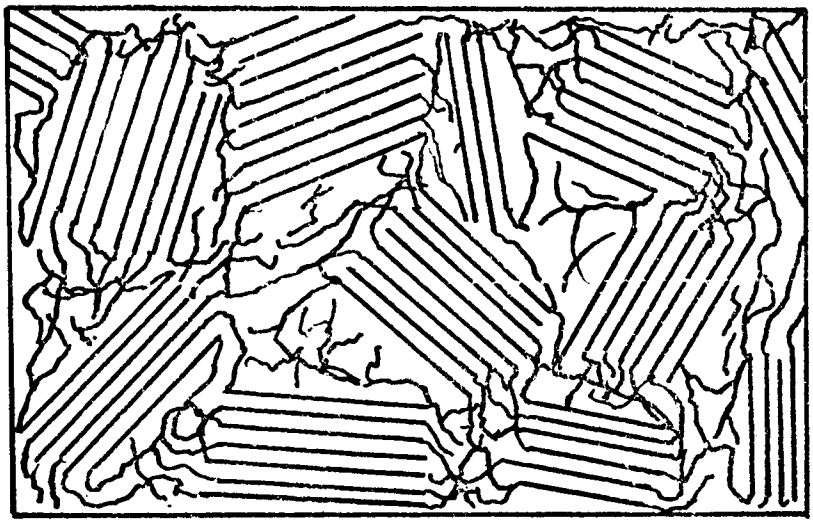


Figure 1. Diagram Illustrating the Proposed Fringed Micelle Structure of Semicrystalline Polymers

pass through several crystalline micelles and amorphous regions in a more or less alternating manner. This model could explain many mechanical, thermodynamical, and electrical properties of crystalline polymers.

The observation of longitudinal electron density fluctuations (27) in fibers by small angle x-ray diffraction studies followed by the independent discoveries by Keller, Till and Fisher (16, 29, 63) in 1957 of solution-grown polyethylene, with a thickness of about 100 Å in the chain direction, finally led to the chain-folding model, Figure 2. Further investigations have shown that folded chain crystals, in the form of lamellae, occur even in melt crystallized polymers. In such materials the folding is probably not as regular as is shown in Figure 2. When many such melt grown crystals are nucleated at a single point they form spherulites in which the lamellae are long radiating and helically twisted ribbons. In the folded chain model, the amorphous component is not a separate phase independent of the crystals; it consists of crystal defects, voids, chain folds including loose loops, free chain ends and tie molecules. Fisher (17) and Statton (57) have observed edge and screw dislocations in polymer crystals. Tie molecules connecting adjacent crystal lamellae are believed to play an important role in determining the mechanical properties of crystalline polymers (7). The number of tie molecules is thought to depend on the crystallization rate (38).

B. PLASTIC DEFORMATION OF SEMICRYSTALLINE POLYMERS

Drawing of Fibers

The fiber as spun usually has a low degree of anistropy, a

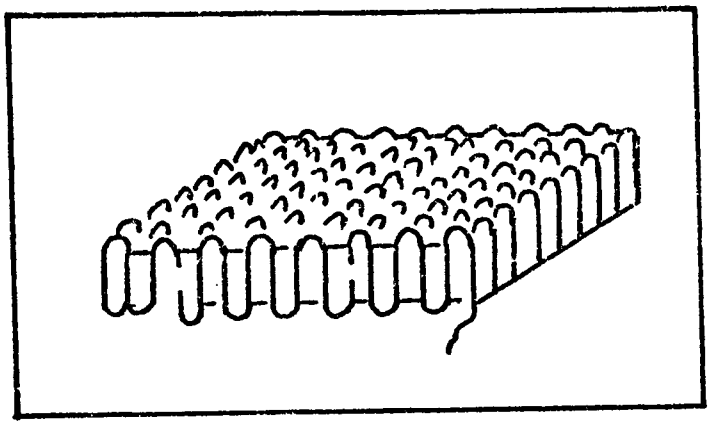


Figure 2. Diagrammatic Representation of a Portion of a Lamellae Crystallite with the Polymer Chains in a Regularly Folded Array

relatively unoriented molecular state, and the mechanical strength is low. By means of the drawing process this structure is transformed into the highly anistropic fiber structure with polymer chains aligned with the fiber axis and high longitudinal elastic modulus and tensile strength.

Necking Phenomenon During Cold-Drawing. During the cold-drawing process, polymeric fibers usually form necks and shoulders (unnecked regions). The cross-section is reduced in a localized region which then travels along the length of the sample. This phenomenon was first observed by Carothers and Hill (8) in 1932. Many attempts have been made to interpret the necking phenomenon from a structural as well as a phenomenological point of view. Marshall and Thompson (33) presented the adiabatic theory of polymer drawing and suggested that necking occurs because of local heating and subsequent softening of the material. Lazurkin (31) observed necking in an amorphous polymer, polymethyl-methacrylate. This indicated that necking phenomenon are not confined to crystalline polymers. Robertson (43) and Barrwens (5) developed a theory of necking with the purpose of interpreting the draw rate dependence of necking stress. Recently, White, Dharod and Clark (61) investigated the interaction of melt-spinning and drawing variables of polyethylene fibers. They observed that the high density polyethylene fibers exhibited necking on cold-drawing but not the low density poly-ethylene fibers.

Voids and Orientation in Drawn Fibers. Void formation during drawing was discovered early and it was implied experimentally that it

was the main cause of reduced density in drawn fiber. Bertleheim and Stein (6), and later Glenz, Peterlin, and Wilkes (21) observed a decrease in density during cold-drawing of polyethylene. Morphologically speaking, during the drawing process, variations in the size of voids depend on the crystalline and amorphous nature of the material and the drawing condition. Samuels (50) used dark field electron microscopy and found microvoids in drawn polypropylene fiber, suggesting that deformation was accompanied by void formation. Recently, White, Dharod and Clark (61) have also observed the decrease in density of polyethylene fibers due to cold drawing.

One of the most dominant features of drawn fibers is the development of molecular orientation. Fankuchen and Mark (15) described the orientation in necked and unnecked regions of cold drawn nylon. Stein and Norris (59) found the amorphous as well as crystalline regions oriented on stretching low density polyethylene fibers. Orientation was determined by x-ray diffraction combined with birefringence and infrared dichroism. They believed that amorphous chains are stretched after sufficient drawing. Samuels (50) observed the increase in Hermans orientation function on drawing polypropylene. The c-axis orientation function (chain direction) ranged from 0.5 to 0.9 at draw ratios of 1.0 and 4.0, respectively. It should be noted that perfect alignment of the c-axes with the fiber axis corresponds to a value of 1.0 for the orientation function. Recently, White, Dharod and Clark (61) determined the Hermans-Stein orientation factors f_a, f_b and f_c for both as-spun and drawn polyethylene fiber. For drawn fibers which contained necks, patterns were made in both the necked and unnecked

regions. In the unnecked region f_a and f_c are still determined largely by the spinning conditions. In the necked region, f_c has a value of 0.95 or greater and f_a and f_b is about -0.45 which indicates nearly perfect axial c-axis crystalline orientation.

Annealing of Drawn Fibers and Drawing at Elevated Temperature. Geil (20) mentioned that the annealing process increases the thickness of lamellae. It is accompanied in many cases by the development of large voids at the spherulitic centers but the size of the spherulite does not change. Matsuokas (34) and Peterlin (39) have both reported that during annealing the density of the polyethylene first decreases and then increases again.

Andrichenko and co-workers (3) carried out structural studies on polyethylene fibers stretched at 100°C. They concluded that structural changes during drawing take place in two stages: Recrystallization and gradual orientation of crystallites along the fiber axis take place during the first stage of deformation up to draw ratios of eight to one. Reduction in long period from 220Å to 173Å was observed during this stage. During the second stage (fibers drawn beyond 800 percent) intrafibrillar structural changes take place but orientation remained unchanged. Later Muzzy and Hansen (36) carried out an investigation on structural change taking place during the drawing of polyethylene rods at 60°C and 100°C. They concluded that disruption of spherulites occurs during the early stage of neck formation which is then followed by formation of an oriented fibrillar structure.

Fibril Formation in Drawn Fibers. With the introduction of

commercial electron microscopes, fine fibrils were observed in synthetic fibers. Extensive investigations on the morphological changes in the transformation from a spherulitic into a fibrillar structure have been conducted by Peterlin and his co-workers. These investigations have led to a generally accepted model of the spherulitic to fibrillar transformation. This model is shown in Figure 3. Peterlin and Balta-Calleja (40) state: "Macroscopically, one hence observes in the neck a gradual transformation of the spherulitic structure into a fibrous structure although the individual untramicroscopic process is discontinuous as in the case of the microfibrils pulling out of single crystals." Peterlin's model as developed is based primarily on observations of high density polyethylene (35, 63) but has been shown to also apply to low density polyethylene (41) and to certain polypropylene samples (44).

Sakaoku and Peterlin (47) described additional features of the model. The decisive step in the plastic deformation of a microspherulitic structure into a highly oriented fiber structure is the complete destruction of every lamellae of the original structure through "micro-necking." During deformation micro-necks occur at cracks which cut through a sufficient number of chain folds. The chains do not rupture but bridge the gap, partially unfolding and tearing off folded-chain blocks which are incorporated into microfibrils of the new structure. The unfolded-chain sections form intrafibrillar tie molecules which are mainly responsible for the high longitudinal strength of the new fiber structure (49).

Meinel and Peterlin (41) explained that strain hardening in the stress-strain curve of a fiber is due to extending interfibrillar tie

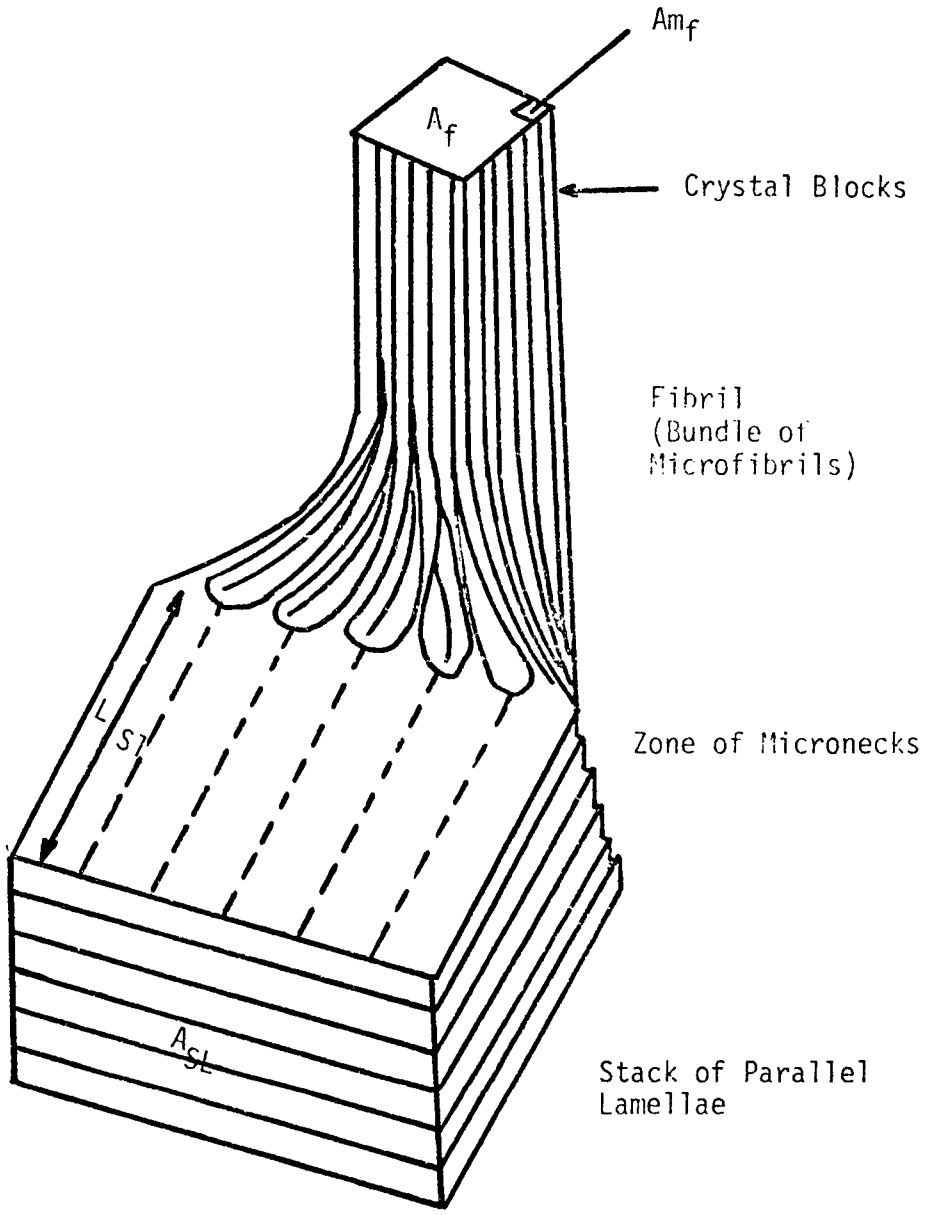


Figure 3. Peterlin's Model of Transformation from a Spherulitic into a Fibrillar Structure

molecules which connected adjacent lamellae in the undeformed, micro-spherulitic material. Slippage of fibrils has been proposed and discussed by O'Leary and Geil (37) and by Robertson (45). Samuels has done extensive work on characterizing the deformation of initially spherulitic isotactic polypropylene (48, 49). He did not emphasize fibrillar formation but his brief descriptions were similar to those of Peterlin.

Twisting of Fibers

Little comprehensive work on the subject has been reported. Most of the earlier work involved twisting at constant load. Dent and Hearle (14) studied the tensile properties of twisted single fibers. They reported that both the tenacity and the extension at break decrease with the increase of twist and all fibers respond in a similar manner. Later, Prevorsek and Lyon (42) showed that both temperature and degree of orientation have an appreciable effect on the force extension properties of twisted fibers. Cooper, McKinnon, and Prevorsek (10) studied the twisted drawn nylon 6 and polyethylene terephathalate (PET) fibers. They (11) also compared morphological changes of twisted nylon 66 and PET fibers. They observed that with twisted nylon 66 fibers, the (010) reflection is split into a bimodel intensity distribution about the equator. Recently, Hein, Cooper and Koutsky (25) investigated the morphology and mechanical properties of four different twisted fibers--polyethylene, polypropylene, nylon 66 and polyethylene terephathalate. On untwisting, they observed that the total recovery of the twisted polyethylene fiber only occurs if the twist angle as

determined by x-ray diffraction is less than about 26 degrees. If the twist angle is greater than this value, the (hk0) planes do not return to the initial orientation.

Transverse compression will occur during the twisting of fibers. Frank, Keller and O'Connor (18) interpreted the rolling texturing of drawn polyethylene in terms of mechanical twinning and slip. They also referred to extra lines on the x-ray diffraction pattern which were observed for severely cold-worked specimens and suggested a possibility of a martensitic phase transformation due to stress. Seto and co-workers (53) investigated oriented polyethylene under transverse compression. Changes were interpreted in terms of twinning, slip and phase transformation to a monoclinic form. The space lattice of monoclinic form has $a = 9.09$, $b = 2.53$, $c = 4.79\text{Å}$ and $\beta = 107.9°$. In 1964, Kiho, Peterlin and Geil (30) published their excellent study on the deformation of single crystals of polyethylene deposited on a mylar substrate; they have shown several modes of deformation including phase transformation very clearly. Hein, Cooper and Koutsky (25) found (200) arc splitting in their highly twisted polyethylene fibers and explained these effects in terms of phase transformation to the monoclinic form.

On twisting or untwisting of fibers, when one portion of a crystal shears relative to the materials on either side of it, a kink band is formed. In the case of metal, kinking is observed when a compressive shearing force acts normal to a single operable slip plane. For polymers, Zaukelies (65) reported the observation of kink bands on the surface of nylon 610. Robertson (44) found that kink bands often develop and grow, when oriented polyethylene is sheared at an angle

to the orientation axis. Seto and Tajima (52) found three kinds of kink bands and suggested that grain boundaries in polymers play an important part in the formation of the kink band. Later, Robertson (46) studied high density polyethylene and isotactic polypropylene with a newly designed shearing device. He found kink bands were initiated at sites of shear stress concentration where the fibrils are first deformed into an s-shaped curve that then tightens and finally collapses into kinks. Hein, Cooper and Koutsky (25) found that the surface of polyethylene fiber exhibits endless stacks of kink bands generally perpendicular to the fiber axis when the fibrils are forcibly untwisted back to the initial state. The x-ray pattern of a highly oriented drawn fiber contains a series of slightly elongated spots on the equator. When the fiber is twisted the intensity in the spots tends to spread out in the azimithal direction as shown in Figure 4. An idealized model for interpreting x-ray patterns of twisted drawn fiber has been suggested by Cooper, McKinnon and Prevorsek (10). They considered the drawn fiber to consist of crystals which behave independently of one another and which are perfectly oriented with the c-axis parallel to the fiber axis. The fiber was divided into a series of annular regions of equal mass. On twisting, the c-axis in any annulus undergoes a helical distortion as shown in Figure 5 with tilt angle:

$$\phi = \arctan(2\pi rt) \qquad (1)$$

where r is the radius of the annulus and t is the twist in turns per unit length. Each crystal on twisting rotates around a fiber radius

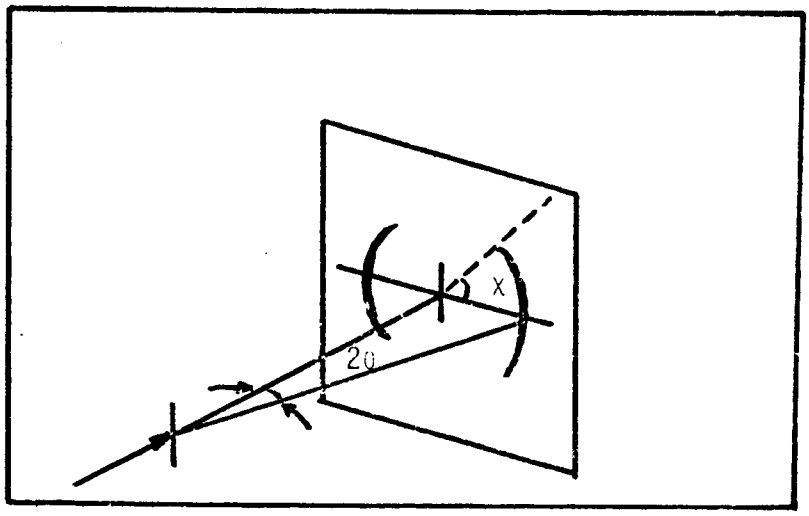


Figure 4. Schematic of X-Ray Diffraction Patterns Showing 2θ and χ

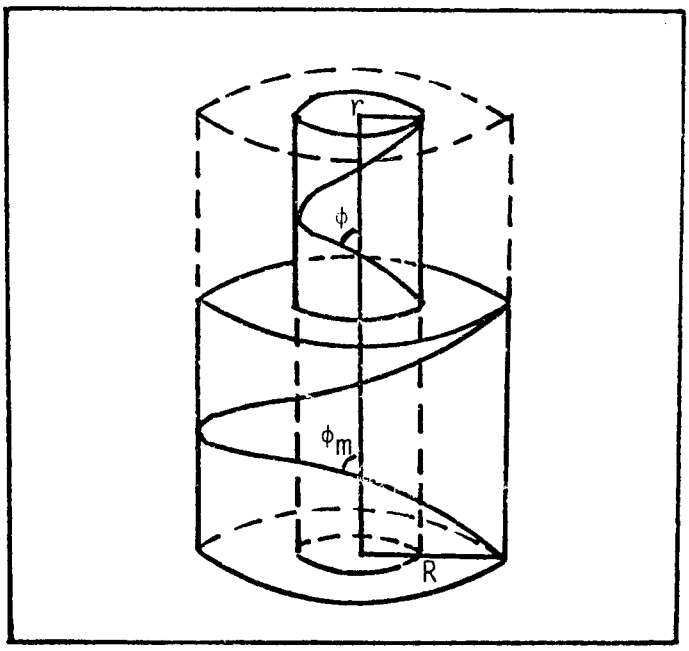


Figure 5. The C-Axis Tilt Angle ϕ and ϕ_m on the Annuli of Radius r and R_m

such that each crystallographic plane rotates in the same manner, keeping its angle β, Figure 6, with the radius unchanged. As a direct consequence of this affine mode of tilting, on the annulus ϕ, a crystallographic plane at angle β with the radius will change from the perfectly vertical position to a tilt angle ϕ with the vertical axis of the twisted fiber given by (10)

$$\sin \phi = \cos \beta \sin \phi_m \qquad (2)$$

where ϕ_m is the experimentally measurable twist angle at the surface of the fiber. With this expression and the relation between ϕ and the azimuthal angle, χ, on the fiber diagram shown in Figure 4, the intensity distribution in the diffraction arc can be calculated. The calculated intensity distributions obtained by Cooper, McKinnon and Prevorsek were in substantial agreement with the observed distributions indicating that the model is an acceptable one.

C. FALSE-TWIST TEXTURING PROCESS

False-twist texturing is presently the most important commercial process based on twisting fibers. The process (62) is illustrated in Figure 7. In diagram (a), the moving yarn case, the twist inserted in the upstream region where the yarn is coming from is removed as the yarn passes the twisting point or spindle. In diagram (b), the stationary yarn case, the turns inserted above the twisting point and below are of opposite sense. The diagram (c) shows the false-twist texturing process. The yarn travelling in an upward direction comes

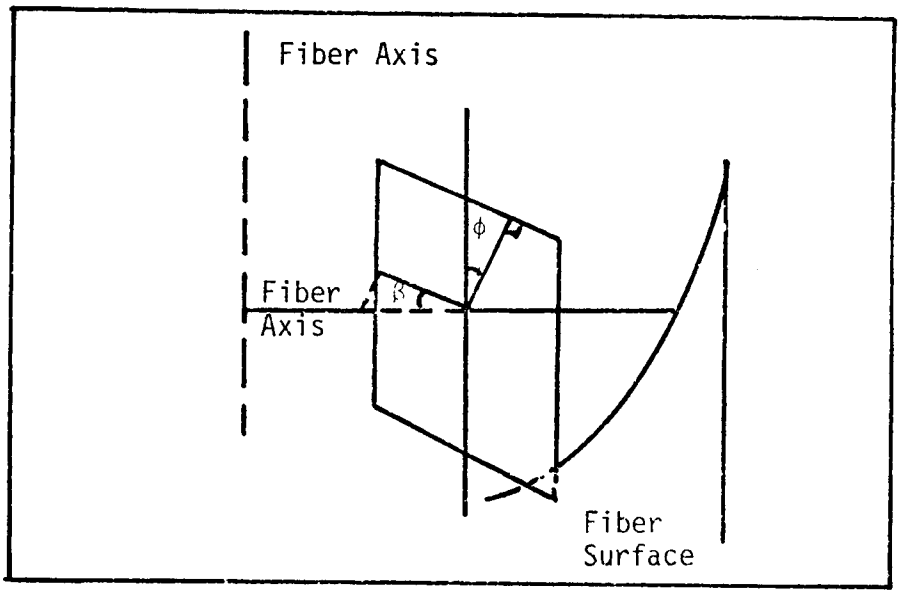


Figure 6. Tilt Angle ϕ and Angle β of a Crystallographic Plane in a Fiber

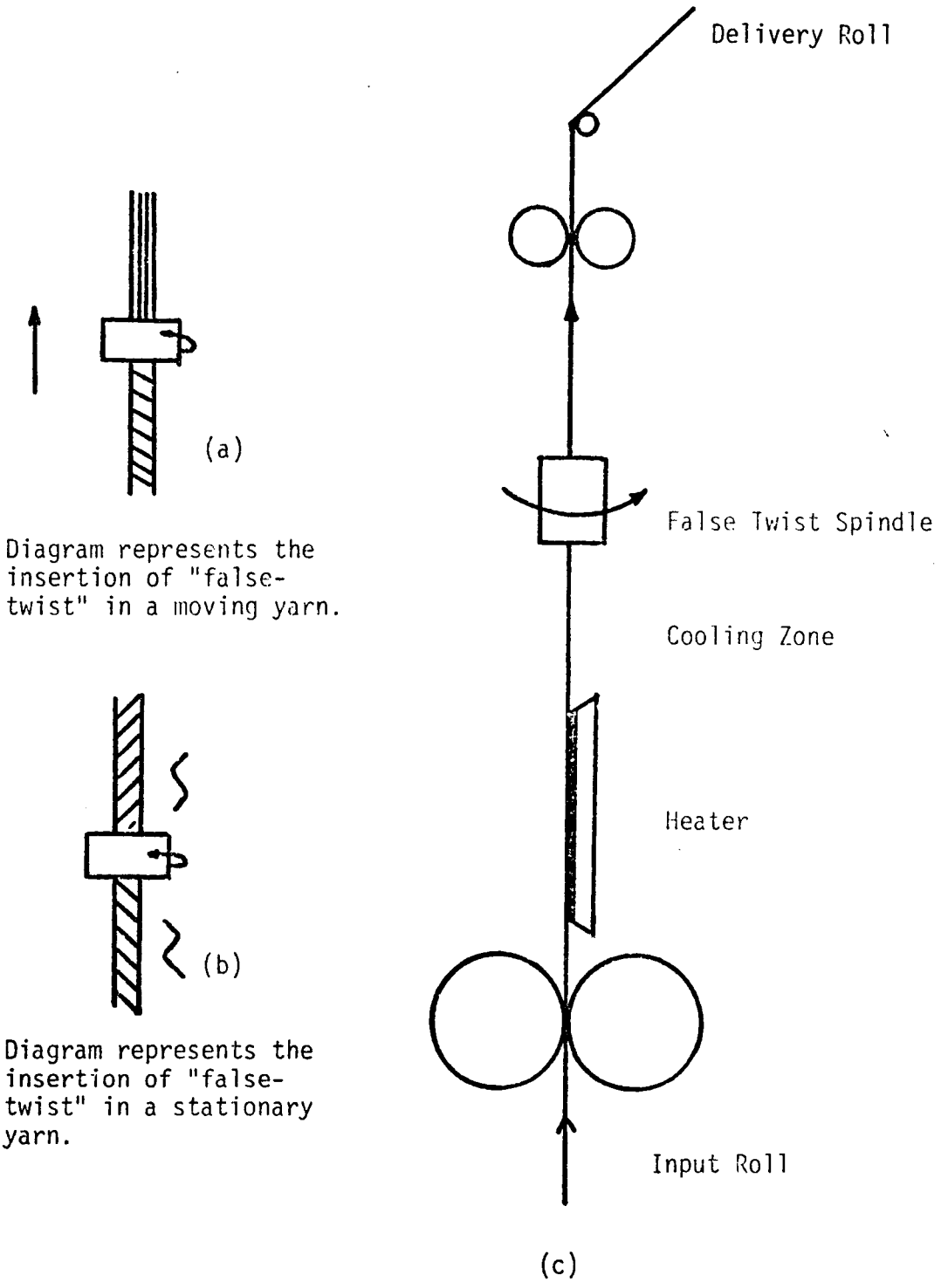


Figure 7. A Schematic Diagram of False-Twist Texturing Principle and Process

under the action of the torque supplied by the rotating spindle when it goes into the system at the input rolls. Here the yarn begins to be cold twisted to a degree dependent on the torque and the mechanical constants of the yarn. Travelling further, it reaches the heating zone; it passes a cooling zone prior to reaching the spindle. It is in these zones of heating and cooling that the setting of the twisted configuration in the filaments takes place. Finally, the yarn passes through the spindle, in keeping with the principle illustrated in diagram (a). The turns that had been inserted temporarily are mechanically removed. At this point, the filaments are forcibly untwisted. Subsequently, the yarn in this stage passes out of the system at the delivery rolls and is wound on a take-up package roll.

CHAPTER III

EXPERIMENTAL DETAILS

A. MATERIALS

Two samples, labeled PE01 and PE07, of high density (linear) polyethylene fiber were chosen for the majority of the research of this study. These samples were previously melt spun in our laboratory by J. R. Dees (13) from Phillips Marlex EMB 6050, lot number 01-2-1308. This polymer had a melt index of 5.0. The spinning conditions for these two fibers studied in depth are given in Table I (see Appendix). Some exploratory work was also carried out on another sample, PE03 (50 m/min) of the same material.

B. COLD-DRAWING

The Instron tensile testing machine was used for cold-drawing of spun fibers. A predetermined length of fiber was clamped between the Instron grips, with the upper grip remaining fixed, and the bottom grip moving downward at a cross-head speed calculated to produce a drawing rate of 50 percent per minute.

C. FIBER TWISTING

A twist tester, manufactured by Alfred Suter Company of New York, was used to twist our fibers at constant load. This device is thirty-three inches long and is shown in Figure 8. One of the two grips was

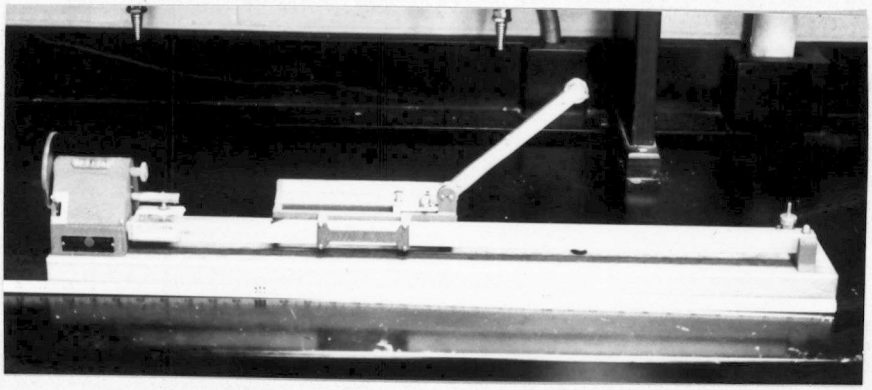


Figure 8. Twist Tester

hooked to a 10 gram load through the use of a pulley. This allowed the grip to move to provide fiber length reduction as twisting proceeds. The other grip was fixed and connected to a twisting handle through a set of gears such that each full turn by the handle caused the grip to make ten full revolutions. A meter, connected to the twisting handle, provided a means for counting the total number of turns.

D. FIBER HEAT SETTING

Fibers were annealed in a temperature-controlled drying oven. All fiber annealing treatments were for thirty minutes at 120°C.

E. SCANNING ELECTRON MICROSCOPY (SEM)

An AMR Model 900 High Resolution Scanning Electron Microscope (Advanced Metals Research Corporation, Burlington, Massachusetts) was used in this study. Observations of both the surface of the spun, drawn, and twisted filaments and the internal structure of "peeled" fibers were made. The fiber peeling technique was first described by Scott (51) in 1959. It is a useful approach for revealing the internal structure of man-made fibers. The fiber is fixed to a glass slide or to a scanning electron microscopy (SEM) sample holder and placed on the stage of a stereomicroscope. An oblique cut is made part way through the fiber with a razor blade as is illustrated in Figure 9. The cut fiber is pulled back parallel to the fiber axis with a pair of sharp tweezers.

A special specimen holder was designed in order to maintain a constant level of twist while observing the surface of the twisted fibers. This holder is shown in Figure 10. The diameter of the ring

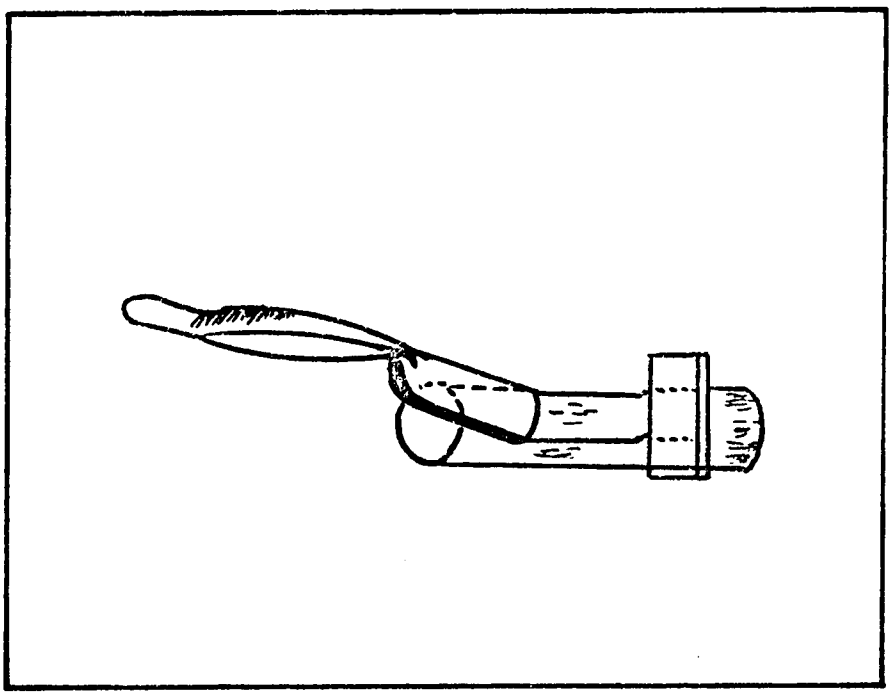


Figure 9. Illustration of Fiber Peeling Technique

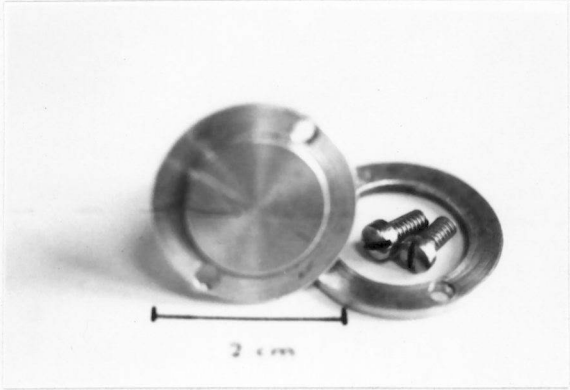


Figure 10. Specimen Holder for Scanning Electron Microscopy

in the picture is 1.5 centimeters and is used for holding the twisted fiber on the holder.

Good mounting and coating of the samples on the holder is necessary to eliminate specimen charging in the electron beam. Figure 11 shows the method of mounting a fiber on the specimen holder. A double-sided adhesive tape (3M Scotch) was found to be suitable. Sikorski (54) had recommended the use of an antistatic (Duron) as the coating material. The disadvantage of using this Duron spray for the fibers was that the coating could not be evenly distributed on the sample, and it was not as effective as metallic coatings in conducting away the charge. A gold-palladium alloy was chosen and applied by evaporation in a Balzers high vacuum coating unit (micro-BA3). The SEM was operated at 21 kv.

F. X-RAY DIFFRACTION STUDIES

Wide Angle X-ray Scattering (WAXS)

Wide angle x-ray experiments were carried out using a Rigaku-General Electric Rotating Anode X-ray Generator. The radiation used was nickel filtered copper K_α of wavelength 1.542 angstroms. The x-ray unit was operated at 50 kv and 80 ma. The sample, which was fixed on the x-ray holder by means of adhesive tape, was 1.85 cm away from the film. The diffraction patterns were obtained on Kodak blue brand x-ray film BB54. Exposures were usually for two hours.

Small Angle X-Ray Scattering (SAXS)

Small angle x-ray patterns were obtained using a custom-made collimator mounted in a Kiessig camera. With the pinholes used in the

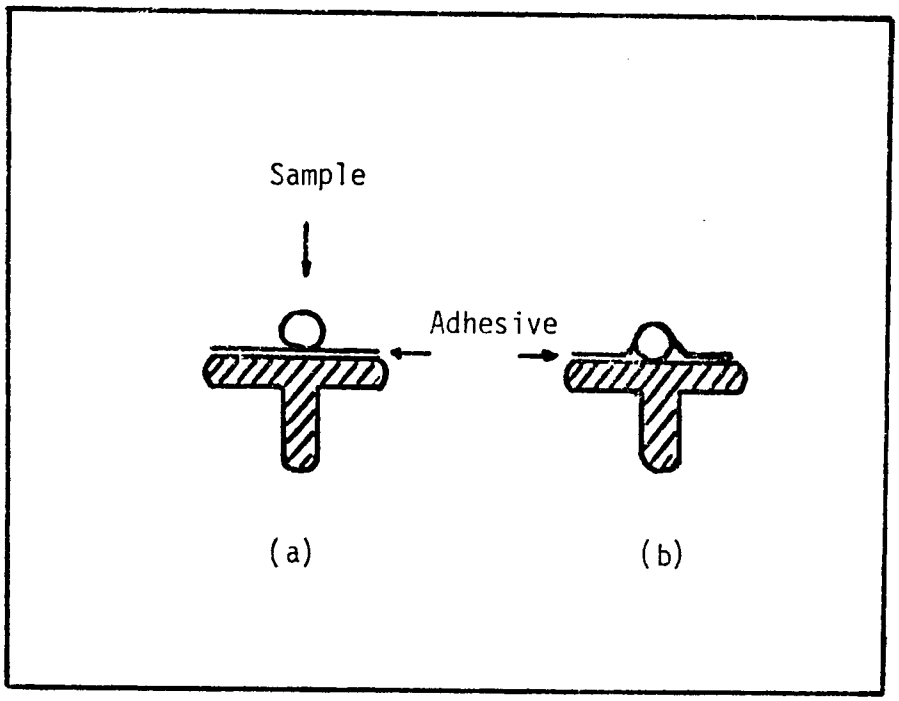


Figure 11. Method of Mounting a Fiber on the Specimen Holder

(a) Incorrect

(b) More desirable since metal coating will be continuous from the fiber to the holder

Source: J. W. S. Herle, J. T. Sparrow and P. M. Cross. Use of the Scanning Electron Microscope, Pergamon Press, 1972.

present work, this custom-made collimator provided a resolution of about 400 angstroms. The camera was evacuated by a mechanical vacuum pump to reduce air scattering. The sample to film distance was 400 mm. The exposure time was in the range of one to two hours because of the high intensity of the x-ray beam used.

G. MECHANICAL PROPERTY MEASUREMENTS

An Instron Tensile Tester (Floor Model) was used to determine the mechanical properties of deformed fibers. To transfer the twisted fibers to the Instron tester and to maintain the twist level, a simple fiber frame (Figure 12) was made. After the fiber was twisted on the twist tester, it was fixed on the frame by adhesive tape and was cut away from the tester by scissors. The fiber on the frame was then transferred to the Instron grips which were one inch apart. The grips were tightened on the length of twisted fiber as indicated in Figure 13. The fiber was then cut away from the frame leaving a twisted section between the Instron grips. This section had the same twist level as it had in the twist tester. Throughout the transfer procedure, extreme care was taken to avoid any slight movement of the grips which would prematurely deform the sample and cause inaccuracies in the measured mechanical properties of the fiber. The fibers were all tested at room temperature at a cross-head speed of one inch per minute.

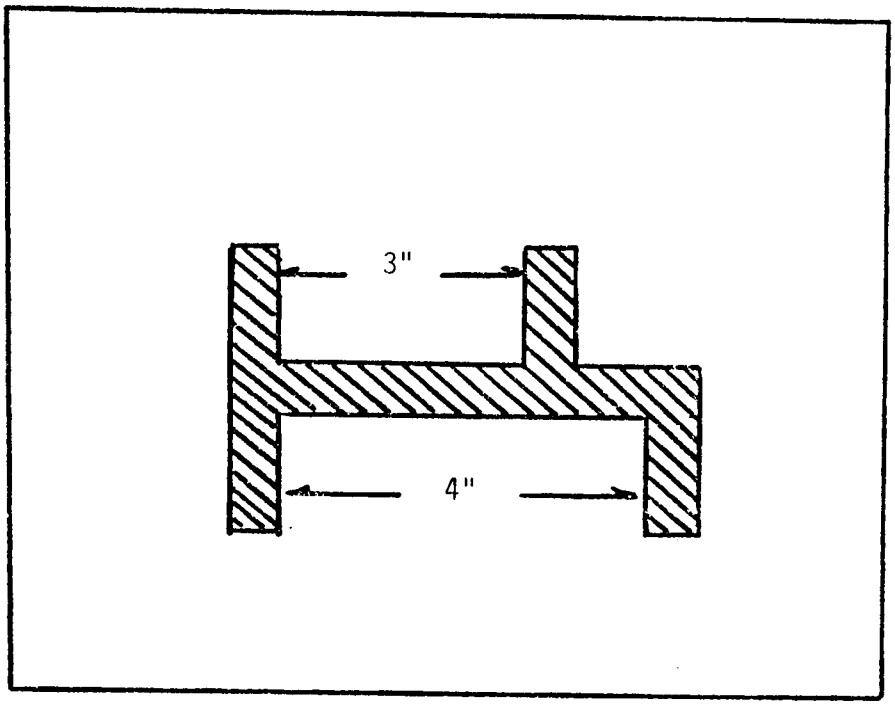


Figure 12. Fiber Frame

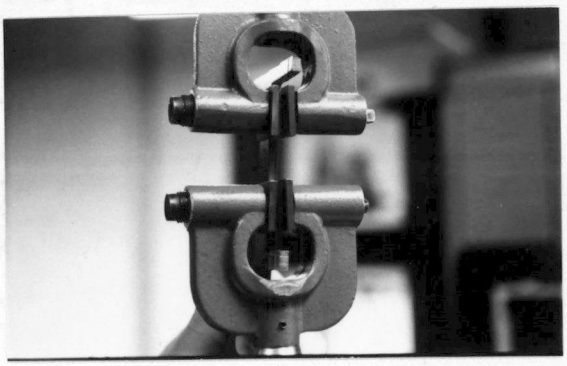


Figure 13. Loading the Twisted Fiber on the Frame to the Instron Grips

CHAPTER IV

RESULTS AND DISCUSSION

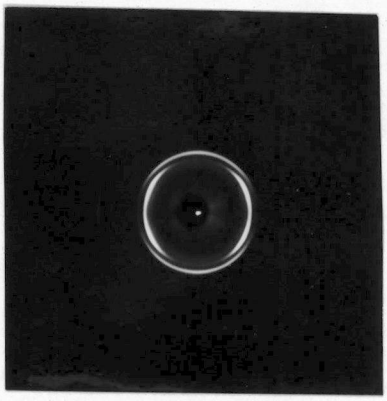
The objective of this research was an experimental investigation of the changes of structure due to deformation of polyethylene fibers. This was accomplished by making wide and small angle x-ray patterns and performing examinations by scanning electron microscopy and testing mechanical properties at each point of the sample treatment sequences presented in Chapter III.

A. AS-SPUN AND TWISTED SPUN FIBERS

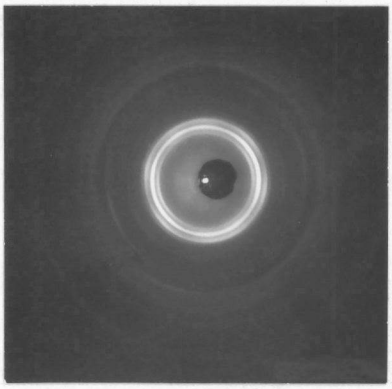
Two fibers of different take-up velocity (PE01 = 100 meters per minute and PE07 = 556 meters per minute) were examined.

X-Ray Studies

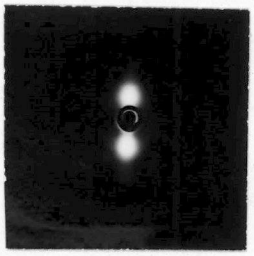
Figure 14 shows the x-ray patterns of the polyethylene fiber with a take-up velocity of 100 meters per minute. The x-ray patterns for the as-spun fiber (a and b) indicate that the orientation in the spun filament is rather high. Note that the (020) reflection is reduced to a short arc on the equator; a fact which indicates that the b axes of the polyethylene crystals are nearly perpendicular to the fiber axis. Dees and Spruiell (12) quantitatively analyzed diffraction patterns from this and other filaments. They obtained values of the Hermans-Stein orientation functions for this sample of $f_b = -0.43$, $f_a = 0.24$, $f_c = 0.19$. According to their interpretation, the morphology



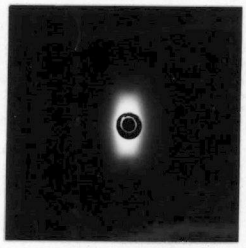
(a)



(c)



(b)



(d)

Figure 14. X-Ray Patterns of HDPE (MI = 5.0) PE01 (100 m/min)

(a) As-spun (WAXS)

(b) As-spun (SAXS)

(c) As-spun, twisted 200 turns/inch (WAXS)

(d) As-spun, twisted 200 turns/inch (SAXS)

of this as-spun filament is a "row-structure" with folded chain lamellae growing radially outward from fibril nuclei which are parallel to the fiber axis. The lamellae apparently twist about the b-axis as they grow outward; a feature which accounts for the nearly equal orientation factors for the c and a axes.

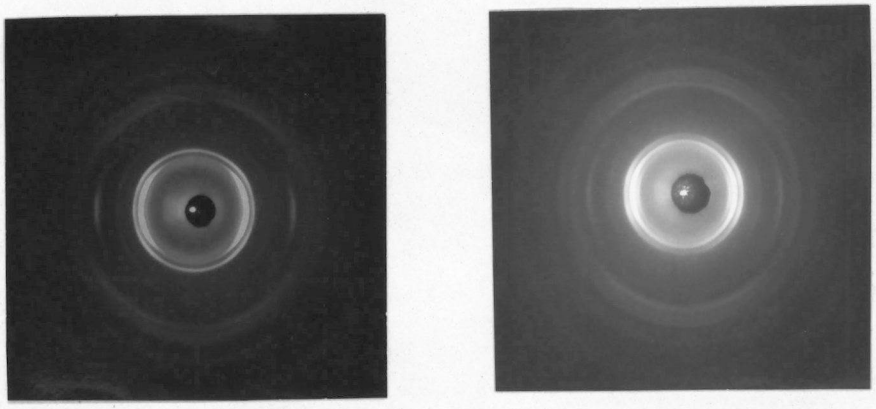
As this spun fiber is twisted up to 200 turns per inch, Figure 14 (c), the intensity spreads more uniformly about the Debye rings, particularly the (110) and (200) reflections. A weak halo or extra ring also appears just to the low angle side of the (110) reflection for the twisted fiber as shown in Figure 14 (c). The precise cause of this ring is uncertain. Since it is broad and is located approximately at the position where the maximum scattering from the "amorphous" component occurs, it might be argued that it represents an extra contribution from the non-crystalline portion of the sample, that is, a decrease in crystallinity with an accompanying increase in order of the amorphous region. This explanation was previously proposed by Slichter (55). It is believed that, while broad, the peak is still too sharp to be attributed to scattering from amorphous material.

A possible interpretation is that it results from the transformation of a small part of the sample to the monoclinic form of polyethylene. This latter interpretation appears to be more likely in view of the fact that the peak becomes more distinct after some treatments to be described later. In these cases the peak clearly arises from a crystalline phase and is located at a diffraction angle identical to the (001) reflection from the monoclinic form of polyethylene. This behavior will be presented in greater detail in a later section of this

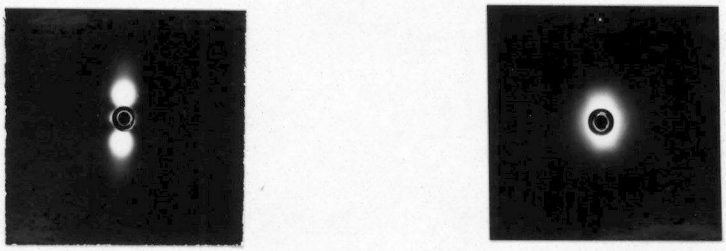
thesis.

The SAXS pattern of Figure 14 (b) exhibits a strong intensity maximum on the meridian with a slight spread of intensity around the incident beam. The meridional maxima is interpreted to indicate that alternating lamellar crystalline and amorphous regions occur along the fiber axis direction and the intensity spread can be associated with a spread in the orientation of the lamellar crystals. This spread is consistent with the twisting of the lamellae described by Dees and Spruiell (12). As for the twisted spun fiber, Figure 14 (d) the meridional intensity and the intensity spread around the incident beam decreases, but there appears to be a very low angle diffuse scattering component superimposed on what is left of the pattern in Figure 14 (b). For all practical purposes the two point diagram in Figure 14 (b) has disappeared. It is assumed that the lamellar crystals and amorphous regions are distorted and disoriented. The diffuse scattering may result from voids opened by the twisting.

For the fiber with a take-up velocity of 556 meters per minute, Figure 15 (a) shows a higher degree of c-axis orientation parallel to the fiber axis and a shift in a-axis orientation such that the a-axes are tending to become perpendicular to the fiber axis. Dees and Spruiell (12) find that $f_a = 0.26$, $f_b = -0.40$, $f_c = 0.66$ for this filament. These results may be interpreted to result from a smaller amount of twisting in the folded chain lamellae than was present in the PEO1 filament. This is also consistent with the small angle x-ray scattering pattern (Figure 15 (b)) which clearly shows a two point diagram without any intensity spread around the incident beam, a fact



(a) (c)



(b) (d)

Figure 15. X-Ray Patterns of HDPE (MI = 5.0) PE07 (556 m/min)

(a) As-spun (WAXS)

(b) As-spun (SAXS)

(c) As-spun, twist 200 turns/inch (WAXS)

(d) As-spun, twist 200 turns/inch (SAXS)

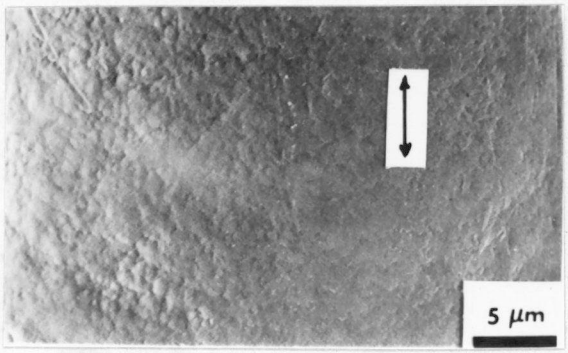
which indicates a fairly regular stacking of lamellar and interlamellar regions parallel to the fiber axis. For the twisted spun fiber, Figure 15 (c) shows that the orientation is again greatly decreased and the halo inside the 110 reflection is enhanced. The SAXS pattern again shows the disappearance of the two point diagram, the reduction of its meridional intensity and the superposition of a diffuse component. Some of the spread in the intensity about the incident beam may result from the change in orientation of lamellar crystals.

Scanning Electron Microscopy

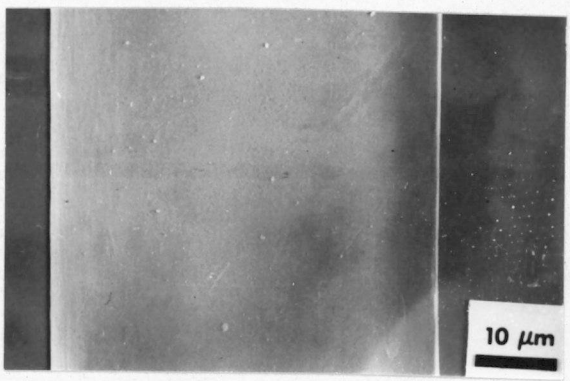
Figure 16 compares the micrographs of as-spun high density polyethylene fibers with different take-up velocities, namely PE03 (50 meters per minute) and PE07 (556 meters per minute). It is interesting that the surface of the fiber with the lower take-up velocity is very rough while the surface of the fiber with the higher take-up velocity is comparatively smooth. The appearance of these filaments did not change appreciably when twisted. The changes in structure caused by twisting were apparently on a scale which was too small to resolve with the SEM.

Mechanical Properties

The force versus percent elongation curves of filaments spun with the different take-up velocities are shown in Figures 17 and 18. For the fiber with a low take-up velocity, Figure 17 shows a pronounced yield point which gradually disappears as the twist level increases. The tensile strength and elongation to break both decrease as the twist level increases. The disappearance of the yield point results from the fact that plastic deformation of the fiber occurs during twisting. This



(a)



(b)

Figure 16. Scanning Electron Micrographs of HDPE Fibers

(a) PE03 as-spun (50 m/min)

(b) PE07 as-spun (556 m/min)

Double arrow indicates fiber axis.

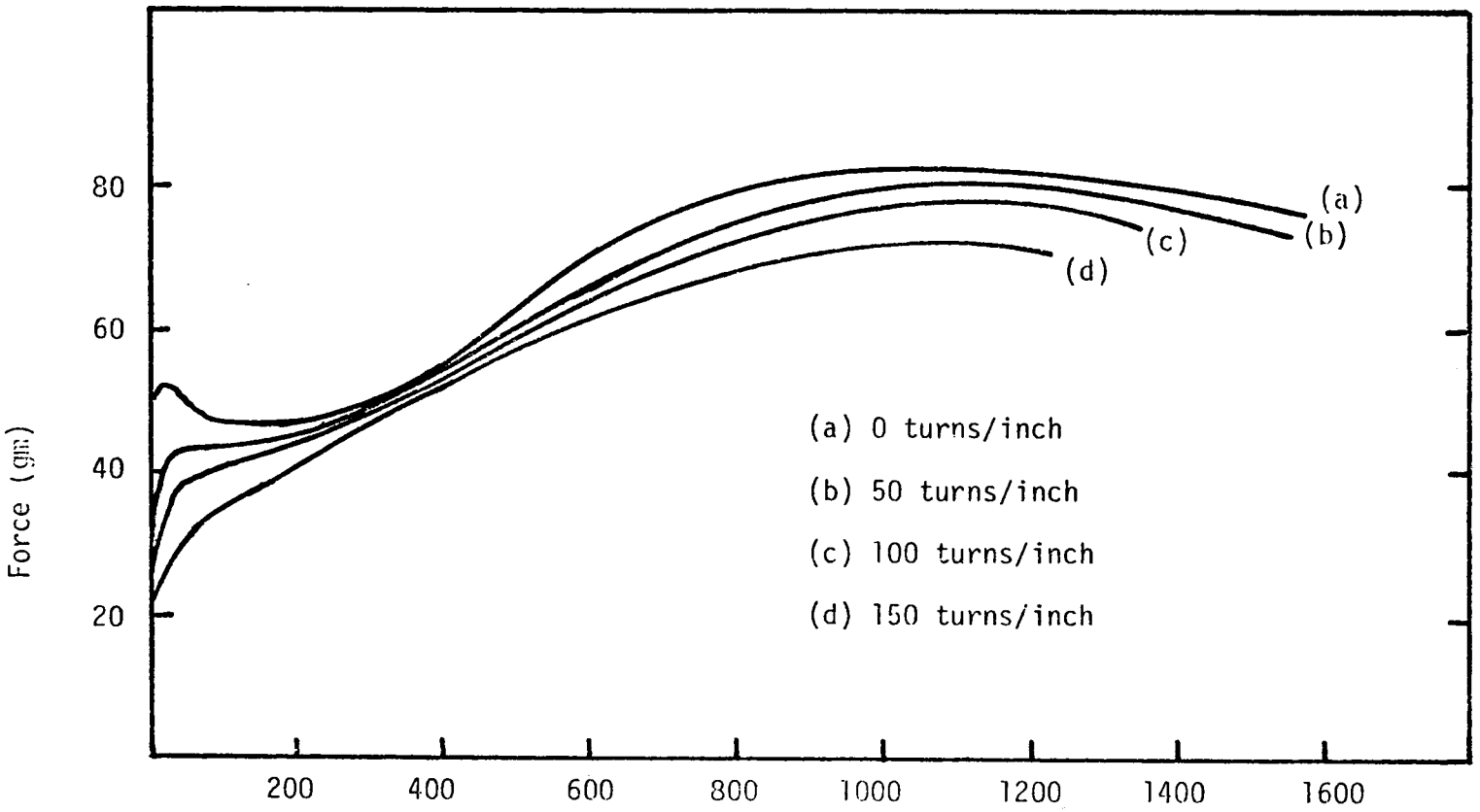


Figure 17. PE01 (100 m/min) Force Versus Percent Elongation at Room Temperature, Twist at Various Degree

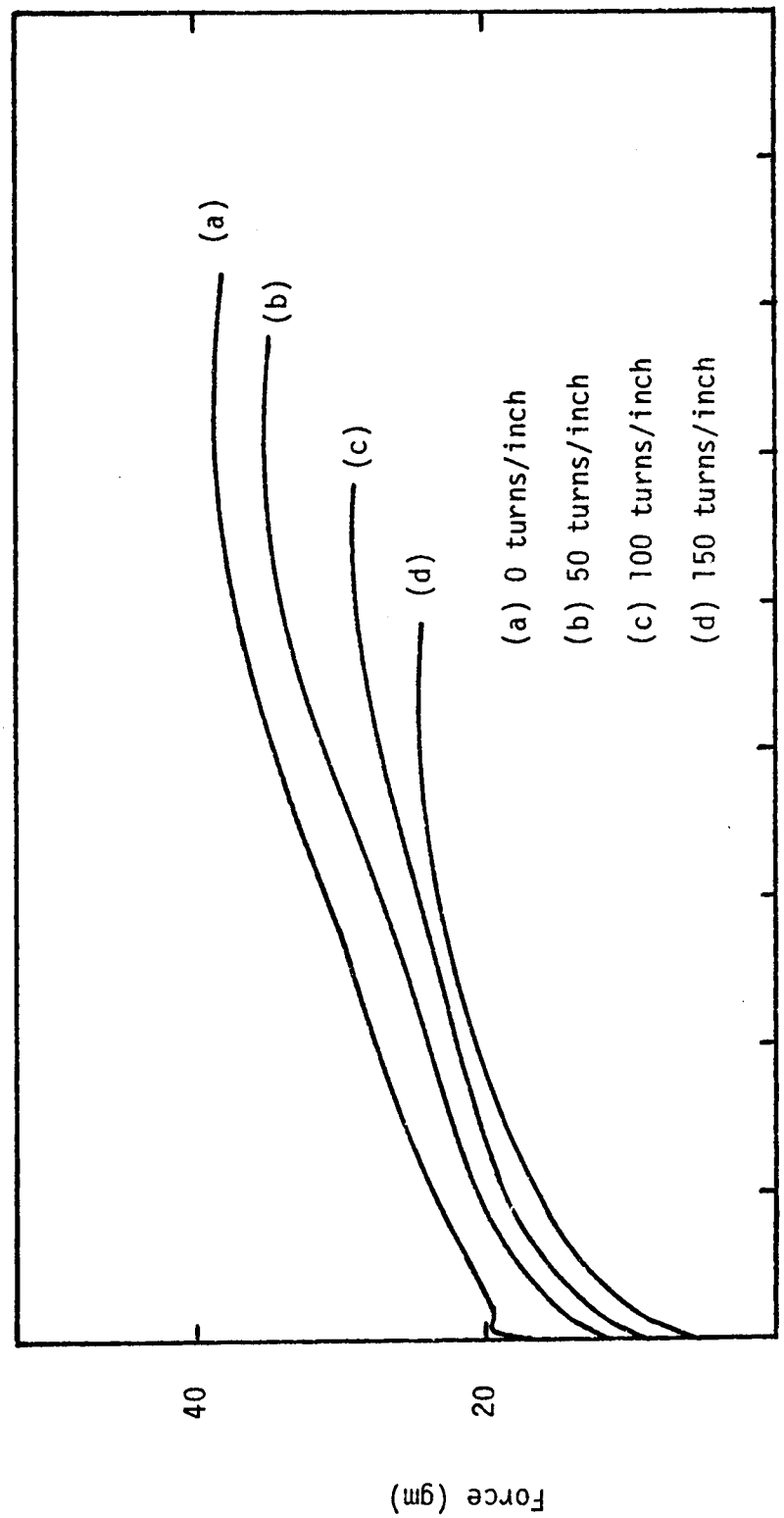


Figure 18. PE07 (556 m/min) Force Versus Total Percent Elongation at Room Temperature, Twist at Various Degree

deformation is uniform over the length of the filament, although it is radially not homogeneous, being greater at the surface than at the center of the fiber. Once a volume element has been stressed sufficiently, it will no longer exhibit a yield drop. Assuming that some critical stress must be exceeded to remove the yield point during subsequent tensile stretching, volume elements near the surface of the fiber will lose the yield point first as twist levels increase. Further increases of twist level will remove the yield point from a greater proportion of the filament cross-section. Accordingly one would thus expect a gradual removal of the yield point as measured on the whole filament. This behavior is indeed observed.

Figure 18 shows force versus percent elongation curve of the fiber with a high take-up velocity of 556 meters per minute. The morphology developed in this filament during spinning results in the near elimination of the yield drop without further processing. It is tempting to conclude that the fiber is partially drawn during spinning due to the higher longitudinal stress. However, there seems to be no other evidence to substantiate such a contention. The tensile strength and elongation to break also decrease with increasing twist in this fiber. Possible reasons for this behavior will be discussed in a later section.

B. DRAWN FIBERS

The drawability, i.e., the ability to elongate the fibers without breakage, of the three melt-spun polyethylenes investigated varied considerably. The PE07 fiber broke at lower elongations than did the PE01 and PE03 elongated under the same conditions. Draw ratio and

percent draw was defined as:

$$DR = L_F/L_o \qquad \text{Percent Draw} = \frac{L_f - L_o}{L_o} \times 100\%$$

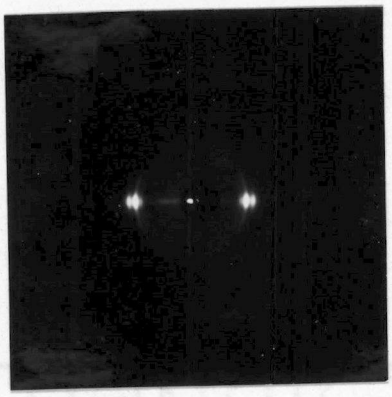
where L_f is the final length and L_o is the initial length. The PE03 fibers spun at 50 meters per minute can be stretched beyond a draw ratio of 20, while the PE01 fiber spun at 100 meters per minute can be stretched beyond a draw ratio of 13. The fiber with a high take-up velocity of 556 meters per minute (PE07) can only be stretched beyond a draw ratio of eight. This clearly shows that the extent of draw before break decreases with increasing fiber take-up velocity.

Necks and shoulders were observed to form during the cold-drawing operation. The draw ratio required for disappearance of necks and shoulders was found to depend on take-up velocity during melt-spinning. For PE03 spun at 50 meters per minutes, a draw ratio of ten was required to make the necks completely disappear, while for PE01 spun at 100 meters per minute, a draw ratio of only eight was required. For the fiber with a high take-up velocity of 556 meters per minute, a draw ratio of only three is required to make the necks completely disappear.

Unless otherwise noted, constant draw ratio was used throughout the investigation of drawn samples. PE01 was drawn 10/1 and PE07 4/1. The exploratory work done on PE03 also was done with draw ratio ten.

X-Ray Studies and Scanning Electron Micrographs

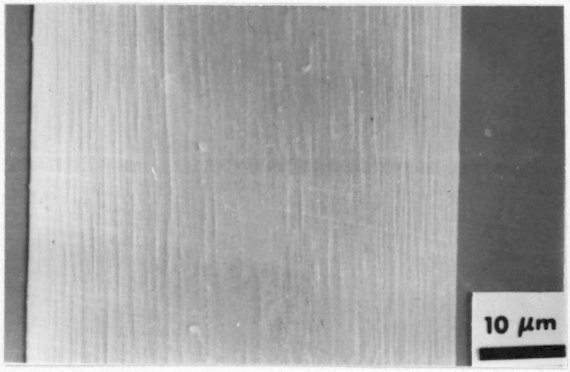
Several qualitative observations can be made from the following diagrams. Figure 19 shows both the WAXS and SAXS patterns of PE01 with



(a)



(b)



(c)

Figure 19. Diffraction Patterns of HDPE (PE01) Fibers and Its Scanning Electron Micrograph

(a) WAXS D.R. 10
(b) SAXS D.R. 10
(c) SEM D.R. 10

a draw ratio of ten. The surface morphology of this drawn sample as observed by SEM is also included (Figure 19 (c)). In Figure 19 (a), the increased level of c axis orientation parallel to the fiber axis and a axis orientation perpendicular to the fiber axis in the final drawn fiber is apparent. The SAXS pattern shows very strong equatorial diffuse scattering with only weak meridional scattering.

Before interpreting the above-mentioned SAXS pattern, some principles of small-angle scattering will be briefly discussed because the exact interpretations of the patterns are still a matter of controversy. In general, the patterns obtained at these small angles from a fiber show two types of effects, discrete diffraction and diffuse scattering.

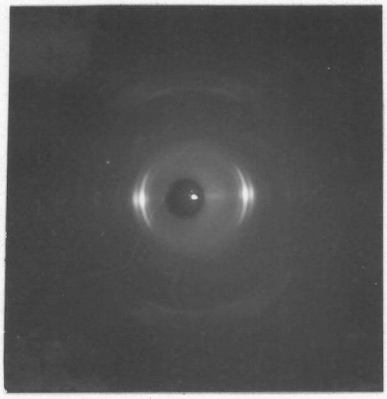
Discrete diffraction at small angles is due to some periodicity of the electron density in the fiber which has a large spacing. Diffuse scattering has maximum intensity at an angle of 0° and decreases in intensity out to 1-2°. It is caused by non-homogeneities of electron density. Unfortunately, the reciprocity principle allows no way of distinguishing between the scattering from a dense particle in a less dense medium and scattering of less dense particles in a dense medium. The scattering from these extreme systems will be equivalent if the density differences are the same.

Hosemann (28) interpreted the equatorial diffuse scattering from fibers. He argued that the values obtained for sizes of non-homogeneities are actually microfibril widths, not the microvoid widths. Statton (56) showed that nearly all fibers show diffuse scattering and argued that this scattering is most likely due to the void content of the fiber.

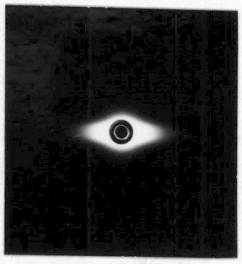
Based on the above-mentioned principles and the previously observed decrease of density of polyethylene during drawing (61), it was concluded that the equatorial diffuse scattering from the present sample (Figure 19 (b)) was caused mainly by microvoids created during the cold drawing steps. If these microvoids are elongated parallel to the fiber axis, the shape of the diffuse scattering is understandable. Returning to the microscopic level, Figure 19 (c) shows that the fibrils on the surface of the drawn PE01 fiber were also parallel to the fiber axis. Voids of the size which are responsible for the equatorial diffuse scattering would be too small to observe at the present magnification using the SEM. There is little doubt, however, that the observed fibrillation results in the necessary microvoids. An additional bit of evidence which supports but does not prove this contention is the ease with which the drawn fibers are "peeled" in the longitudinal direction as shown below. This peeling certainly indicates loss of cohesion and the presence of voids which may be considerably larger than those detected by SAXS.

Figure 20 (a) shows the diffraction patterns of PE07 with a draw ratio of four. It was obvious that the level of c axis orientation parallel to the fiber axis has increased. Figure 20 (b) and (c) show the SAXS and SEM of PE07. Qualitatively, similar results to those shown in Figure 19 (b) and (c) are observed.

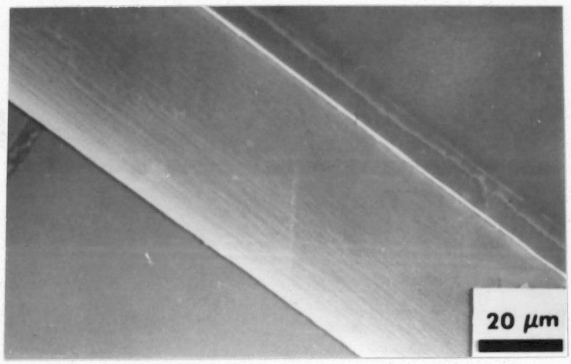
The surface fibrils observed in both pictures (Figure 19 (c) and Figure 20 (c)) stretch parallel to the fiber axis. In order to further investigate the fibrillation, drawn fibers were "peeled" according to the technique mentioned in Chapter II. Figure 21 shows such "peeled"



(a)



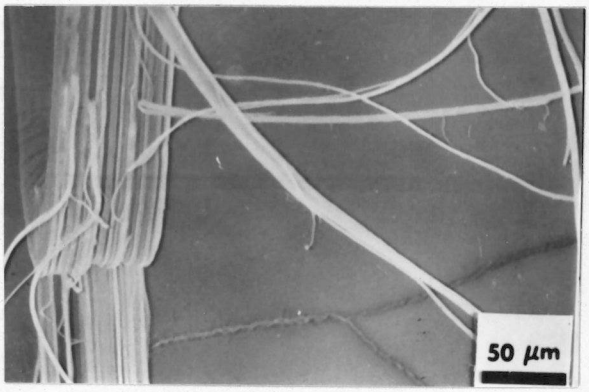
(b)



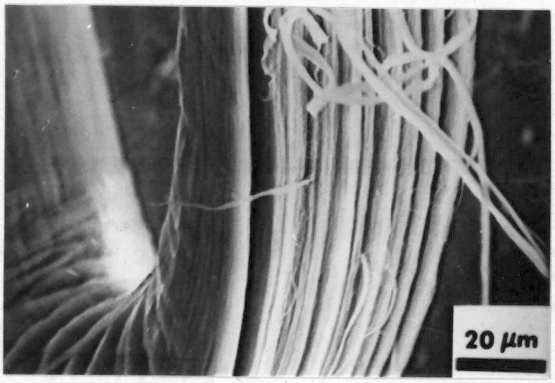
(c)

Figure 20. Diffraction Patterns of HDPE (PE07) Fibers and Its Scanning Electron Micrograph

(a) WAXS D.R. 4
(b) SAXS D.R. 4
(c) SEM D.R. 4

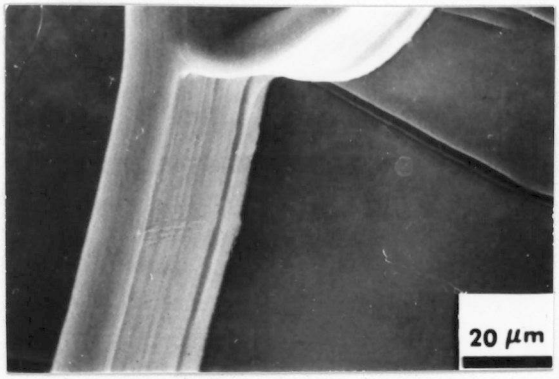


(a)



(b)

Figure 21. Scanning Electron Micrographs of "Peeled" HDPE Fibers



(c)

Figure 21 (continued)

(a) PE03 (50 meters/min) D.R. 10

(b) PE01 (100 meters/min) D.R. 10

(c) PE07 (556 meters/min) D.R. 4

drawn fibers. These peeled fibers revealed a definite fibrillar structure. It is interesting that the fibers with low take-up velocity and high draw ratio (D. R. 10) seem to have a relatively loose bundle of long fibrils (Figure 21 (a), (b)). Comparing the fiber with the high take-up velocity (PE07), there was a lower degree of fibrillation (Figure 21 (c)). This evidence is consistent with the idea that increasing draw ratio causes increased fibrillation. However, it also indicates that at the natural draw ratio or at a given tensile strength level, the degree of fibrillation will be dependent on the melt spinning conditions. Fibers spun at higher take-up velocities will exhibit a lower degree of fibrillation under these circumstances.

Mechanical Properties

The cold-drawing process performed on melt-spun fibers greatly effects the stress-strain behavior of the fibers as shown in Figure 22. The stress plotted in this figure is the "engineering stress" or the load divided by the cross-sectional area of the fiber prior to the test. Figure 22 shows that the stress-strain behavior in both the undrawn and drawn HDPE fibers spun with take-up velocities of 100 and 556 meters per minute. The fibers spun with a take-up velocity of 100 meters per minute were drawn 10/1; necks and shoulders in the fibers were absent upon being drawn 8/1. The spun fibers with a take-up velocity of 556 meters per minute were drawn 4/1; necks and shoulders in the fibers were absent upon being drawn 3/1. The engineering stress at fracture in the drawn fibers was much higher than that in the undrawn fibers. The breaking stress was higher in the 10/1

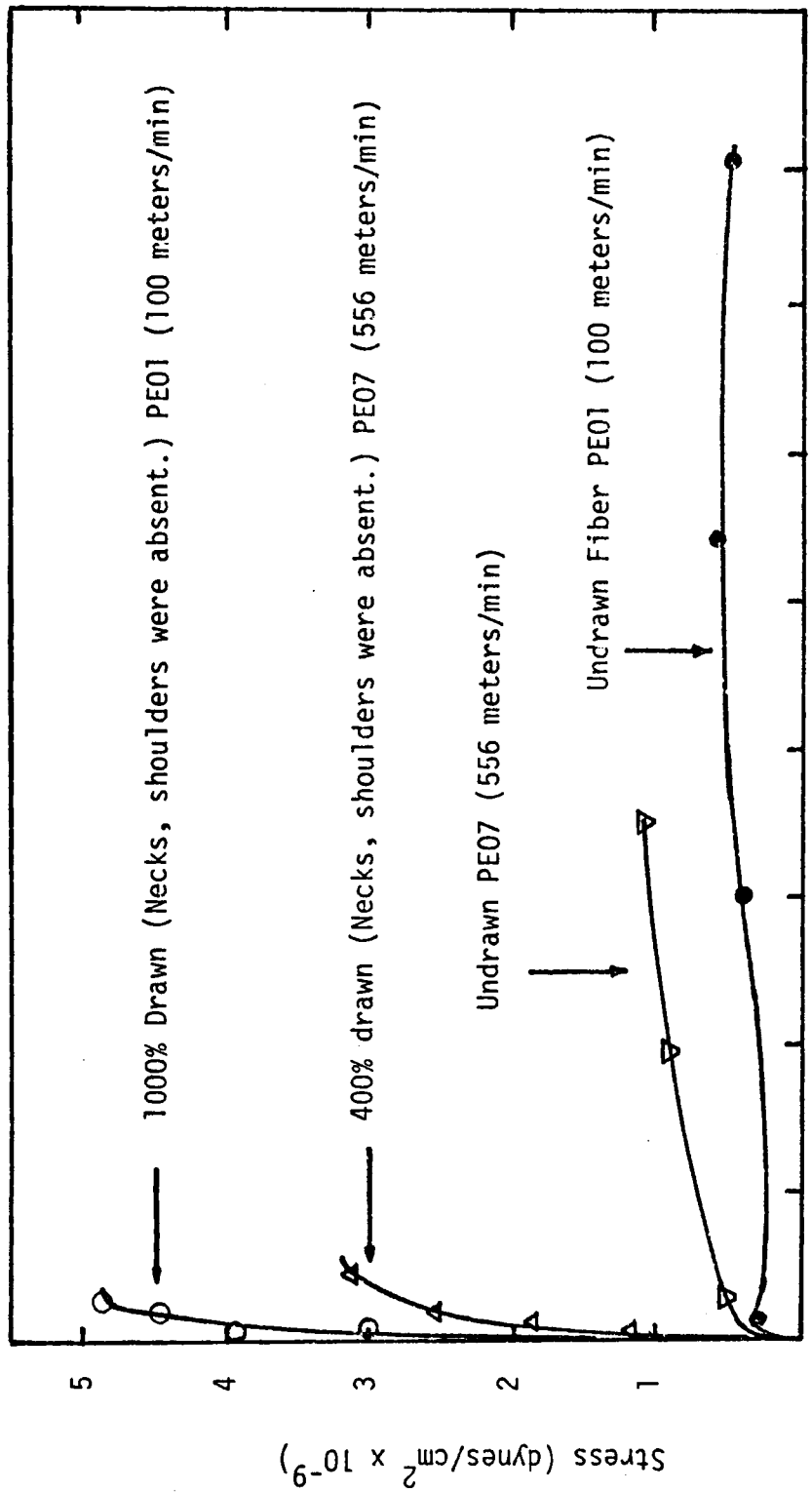


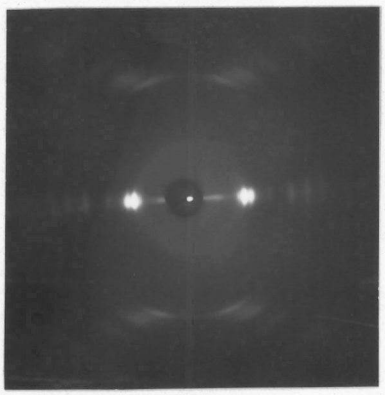
Figure 22. Stress Versus Percent Elongation Curve of HDPE (MI = 5.0)

drawn fibers with a take-up velocity of 100 meters per minute than in the 4/1 drawn fibers spun with a take-up velocity of 556 meters per minute.

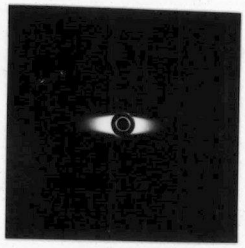
C. DRAWN TWISTED FIBERS

Figures 23 and 24 show the WAXS and SAXS patterns of the PE01 (100 meters per minute) and PE07 (556 meters per minute) fibers after twisting 100 turns per inch and drawing either 10/1 or 4/1. The x-ray patterns of twisted spun fibers were shown in section (A). Here, after the twisted spun fibers were drawn, the WAXS patterns in Figure 23 (a) and Figure 24 (a) clearly show a high c axis orientation parallel to the fiber axis. Comparing this result to that for spun and drawn fibers shown in Figure 6, page 19, and shows that the orientation is little effected by the twisting prior to drawing.

The SAXS pattern (Figure 23 (b)) shows the strong equatorial scattering which means microvoids are also parallel to its fiber axis. The surface fibrils as observed by SEM are shown in Figure 25 (a) and (b). These appear to make a small angle with the fiber axis. This fibril appears to make a small angle with the fiber axis. This effect is particularly noticeable in the PE07 fiber, Figure 25 (b), probably as a result of the lower draw ratio. This effect appears to be caused by twisting prior to drawing; it would appear to indicate that the volume units making up a fibril are well defined in the spun fiber and survive the twisting operation.



(a)

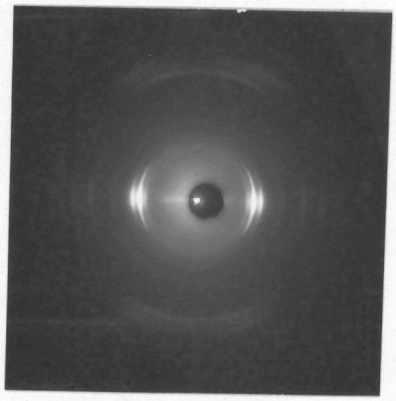


(b)

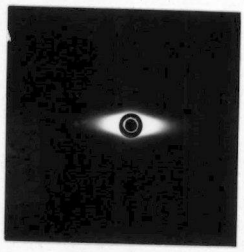
Figure 23. X-Ray Patterns of HDPE (MI = 5.0)
PE01 (100 m/min)

(a) Twisted 100 turns/inch, then draw with D.R. 10 (WAXS)

(b) Twisted 100 turns/inch, then draw with D.R. 10 (SAXS)



(a)

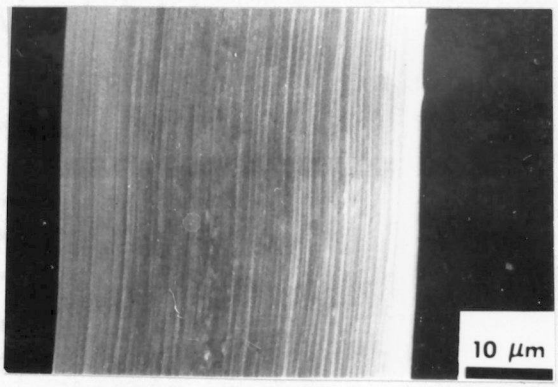


(b)

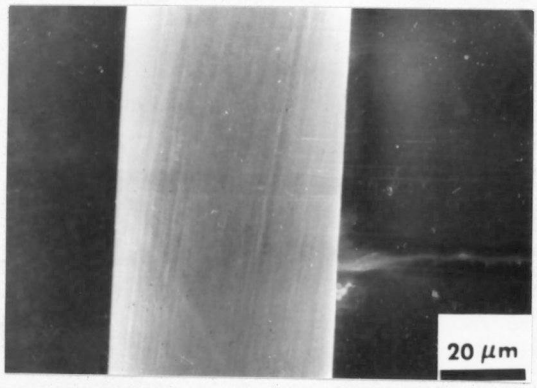
Figure 24. X-Ray Patterns of HDPE (MI = 5.0)
PE07 (556 m/min)

(a) Twisted 100 turns/inch, then draw with D.R. 4 (WAXS)

(b) Twisted 100 turns/inch, then draw with D.R. 4 (SAXS)



(a)



(b)

Figure 25. Scanning Electron Micrographs of Drawn Twisted Fibers

(a) PE01 (100 m/min), twist 100 turns/inch, D.R. 10

(b) PE07 (556 m/min), twist 100 turns/inch, D.R. 4

D. TWISTED DRAWN FIBERS

X-Ray Studies

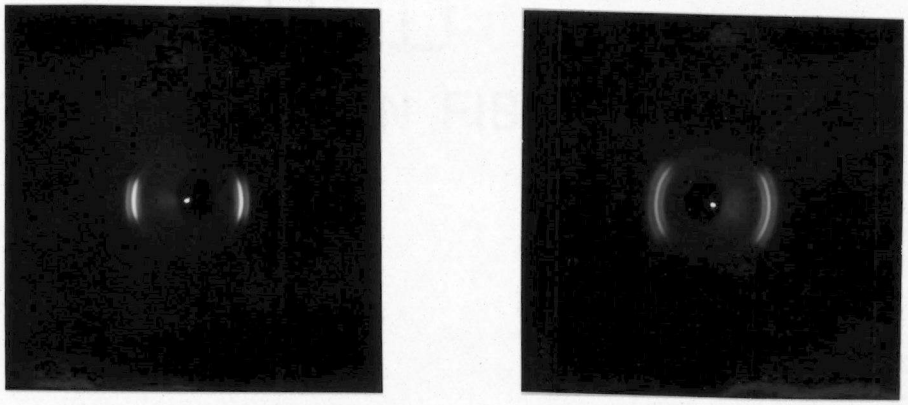
Figure 26 shows both the WAXS and SAXS patterns of PE01 with a draw ratio of ten after twisting 50 and 100 turns/in, respectively. As the twist level increases, the (hk0) reflecting planes on the WAXS patterns (Figure 23 (a) and (c)) become more and more tilted causing the equatorial reflections which are initially spots (compare Figure 19 (a)) to extend into wider arcs. At high twist levels, an extra reflection, not expected on the basis of the orthorhombic unit cell normally encountered for polyethylene and lying inside the (110) arc, becomes quite noticeable.

In the case of the SAXS patterns of the twisted fibers, the distribution of equatorial scattering changed as the twist level increased. The breadth of the scattering normal to the fiber axis decreases, but it fans out parallel to the fiber axis (Figure 26 (b) and (d).

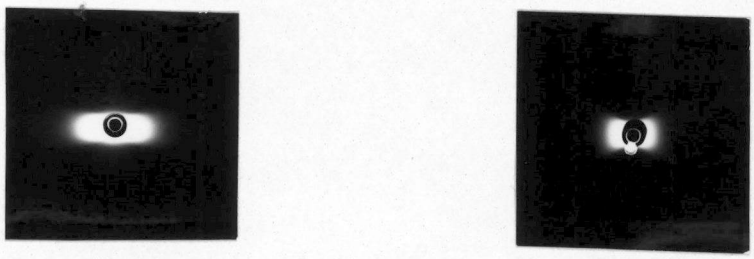
Figure 27 shows both the diffraction patterns of WAXS and SAXS of PE07 with a draw ratio of four after twisting 75 and 150 turns/in, respectively. Similar results to those shown in Figure 26 are observed, including the development of the extra reflection.

On inspection of the WAXS patterns in Figures 26 and 27, it is found that the observed phenomena agreed qualitatively with the affine mode of deformation, described in Chapter II. According to that analysis any equatorial reflection will respond to twisting by gradual lengthening while retaining maximum intensity on the equator.

At maximum level of twist, Hein, Cooper and Koutsky (25)



(a) (c)



(b) (d)

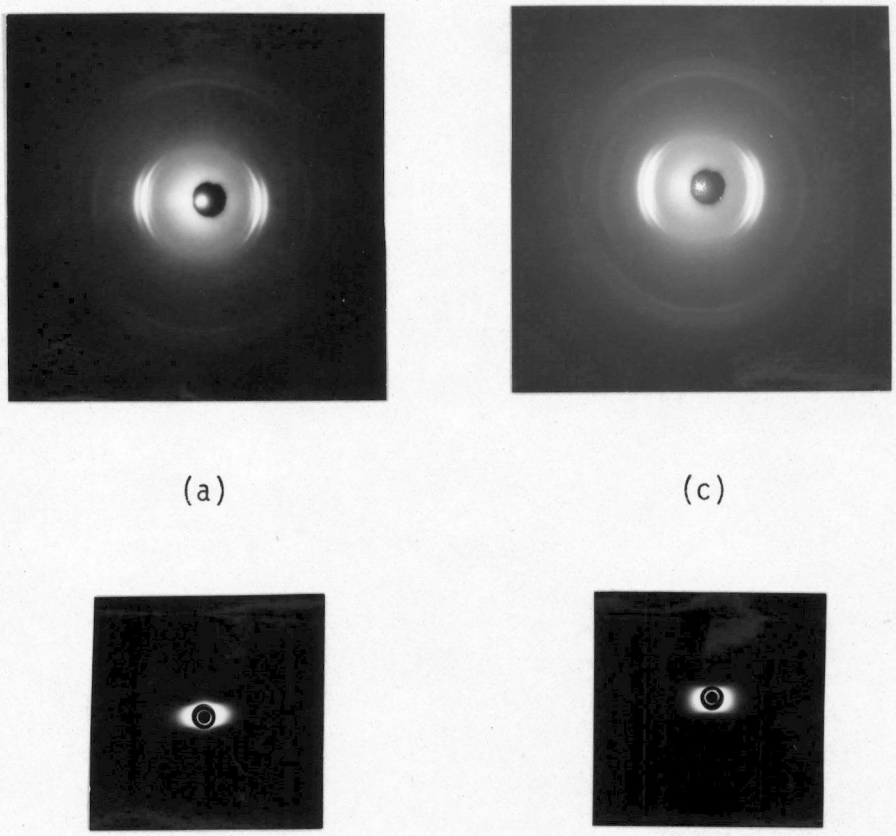
Figure 26. Diffraction Patterns of HDPE (PE01) Fibers (D.R. 10)

(a) WAXS 50 turns/inch

(b) SAXS 50 turns/inch

(c) WAXS 100 turns/inch

(d) SAXS 100 turns/inch



(a) (c)

(b) (d)

Figure 27. Diffraction Patterns of HDPE (PE07) Fibers (D.R. 4)

(a) WAXS 75 turns/inch

(b) SAXS 75 turns/inch

(c) WAXS 150 turns/inch

(d) SAXS 150 turns/inch

observed (200) arc splitting which was not found in our patterns. As was mentioned before, an extra reflection with weak intensity was observed. Measurement showed that the interplanar spacing corresponding to this extra reflection is 4.55Å. This exactly corresponds to the spacing of the (001) planes of the monoclinic lattice described by Seto and Tanaka (53) for polyethylene which has been deformed in compression. It is concluded that the extra reflection in the pattern was most probably caused by a stress-induced phase transformation to the monoclinic form.

According to Frank and co-workers (18), the monoclinic form may be induced by shear stress in a manner similar to that which occurs in the martensitic transformation in steels. Quantitatively, coherent "shear transformation" closely resembles mechanical twinning. A mechanism of this kind is reasonably likely, and would cause rotations of a part of the crystal around the c axis among a number of highly strained lamellae.

The small angle x-ray scattering patterns may be explained on the assumption that the elongated voids, originally parallel to the fiber axis, are tilted by the twisting just as the fibrils are. At the maximum twist levels, the fan or x-shaped diagrams (Figures 26 (d) and 27 (d)) are produced. This explanation agrees well with the interpretation given the WAXS pattern in Figures 26 (c) and 27 (c) that tilting caused the increasing spread of the equatorial arcs.

Scanning Electron Microscopy

As the drawn fiber is twisted, the surface fibrils tilt away

from the fiber axis direction (Figure 28). This result is observed in both samples. Besides this tilting of the fibrils, no other details could be observed.

The maximum tilting of the crystals in the fiber may be estimated from the greatest extent of the arcs on the x-ray patterns. The angle is calculated based on Equation (2) given in Chapter II. The macroscopic twist imparted to the surface layer of the fiber can be directly measured from the maximum twist as observed on the scanning micrographs. Comparisons of these results are found in Table II (see Appendix). It is interesting to note that the macroscopic twist is always greater than that determined from the x-ray pattern.

Mechanical Properties

Figures 29 and 30 show the stress-strain curves of the drawn fibers (PE01 and PE07) at different twist levels. These typical results of constant extension rate stress-strain experiments show that the fiber strength, modulus and elongation to break all tend to decrease as the twist level increases. Two exceptions to this trend occur at small twist angle. Figure 29 shows that the elongation to break at 50 turns per inch is greater than that of the control. A graph showing the relative breaking load versus twist angle is presented in Figure 31. Except for one point, PE01 at 50 turns per inch, the trend of the curves show that relative breaking load decreases as the twist angle increases. Figure 30 shows that in the small twist angle range, the modulus increases slightly over that of the control fiber. This slight increase, also reported by previous investigators (10, 25, 42)

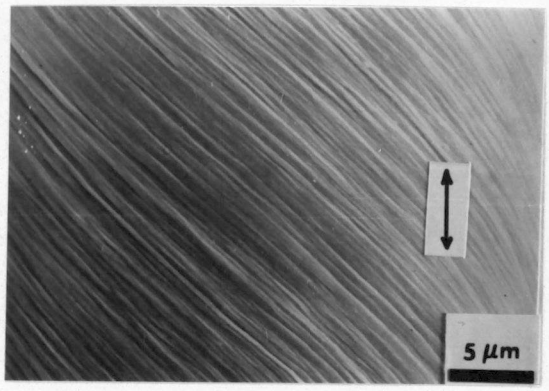


Figure 28. Scanning Electron Micrograph of HDPE Fibers PE01, D.R. 10, Twist 100 Turns/Inch

Double arrow indicates fiber axis.

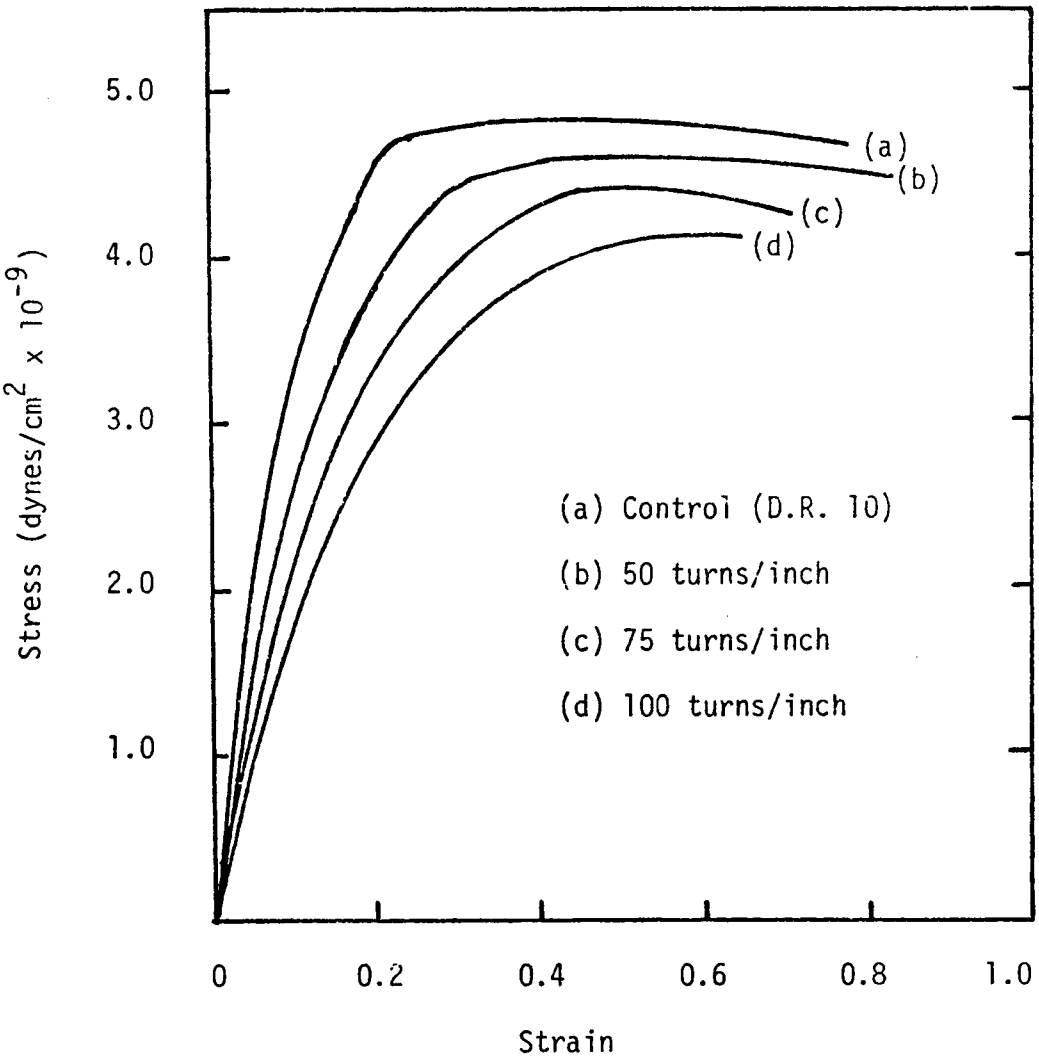


Figure 29. Stress Versus Strain Curve of Drawn PE01 (100 m/min) with Draw Ratio 10, Twist at Various Amounts at Room Temperature

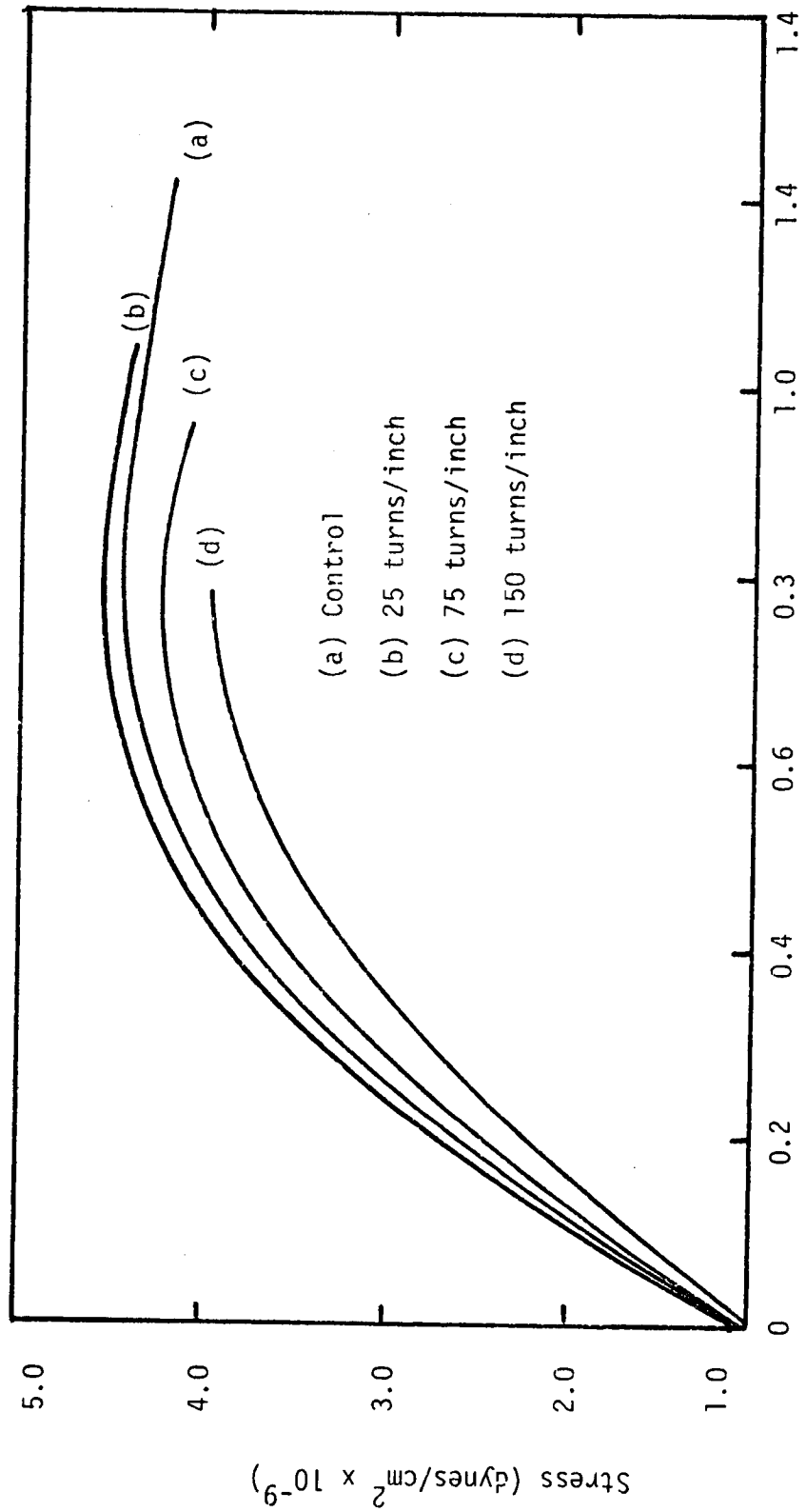


Figure 30. Stress Versus Strain Curve of Drawn PE07 (556 m/min) with Draw Ratio 4, Twist at Various Amounts at Room Temperature

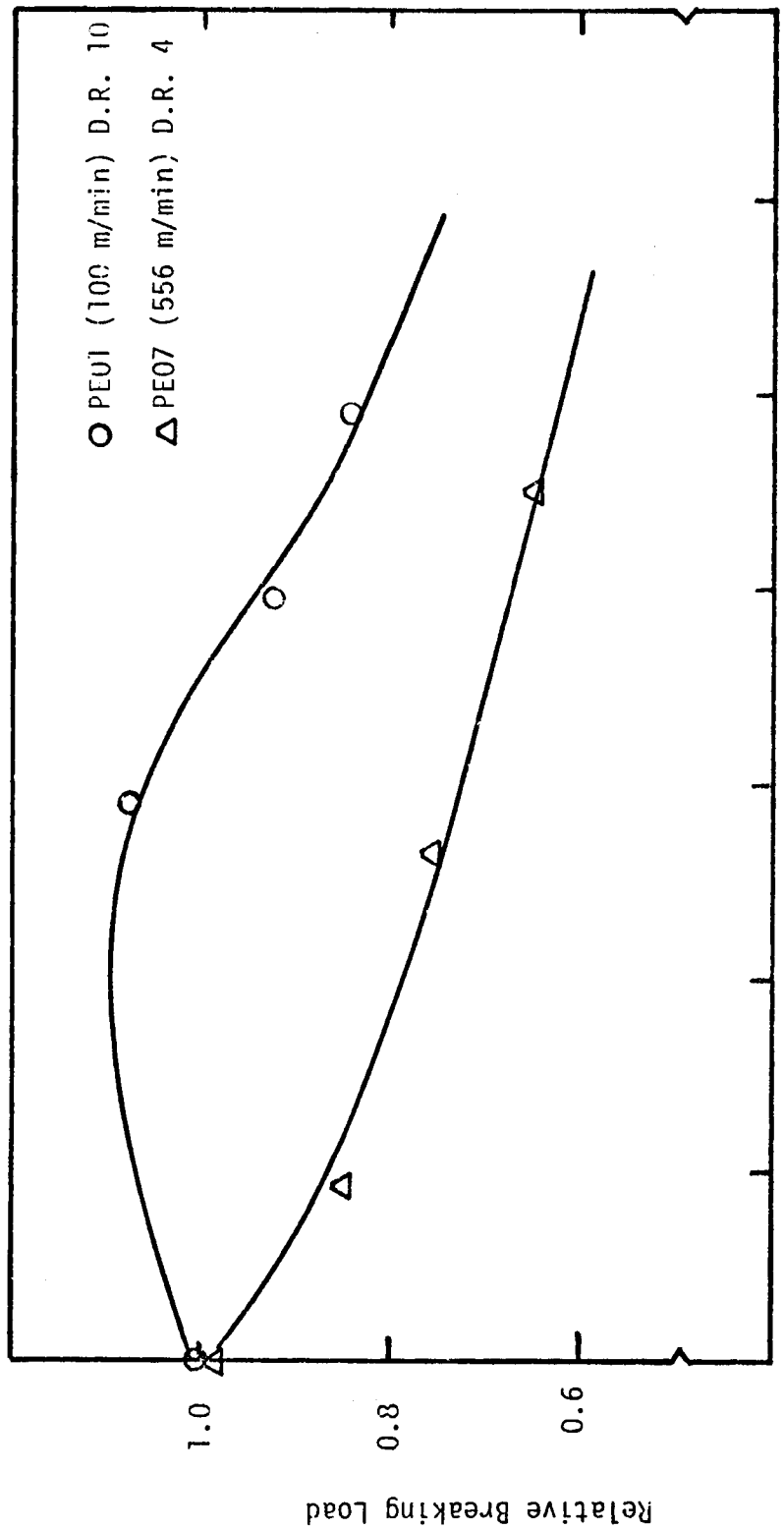


Figure 31. Effect of Twist Angle on Relative Breaking Load of Drawn HDPE Fibers (PEO1 and PEO7) at Room Temperature

has been attributed to the contraction of (secondary) intermolecular bonds resulting in improved lateral packing (42) prior to additional twist. With increasing twist angle, the fibrils themselves undergo considerable spiralling around the fiber axis. This spiralling (10) is not uniform over the whole cross-section of fiber; the distortion becomes more severe as the distance from the fiber axis of the molecular segments becomes greater. Thus, a highly twisted structure would experience considerable lateral rearrangement. This may lead to the formation of cracks, loss of coherency between fibrils and consequently to a decrease in fiber strength and modulus.

Figure 32 shows the effect of twist angle on the relative modulus of drawn HDPE. The relative modulus decreases as the twist level increases. The dotted line in the graph is a plot of $\cos^2\alpha$ where α is the twist angle. The reasonable fit of the data to the $\cos^2\alpha$ curve that is found in Figure 32 appears to be due to the fact that an analogy can be drawn between the twisted drawn fiber and twisted continuous filament yarn. In this analogy the fiber is considered to be made up of fibrils (or microfibrils) just as the yarn is made up of fibers. Gegauff (19), Hearle (24), and others have developed mathematical models for continuous filament yarns to predict their deformation behavior and stress-strain curves. The simplest of such theories predicts that

$$\frac{E_y}{E_f} = \cos^2\alpha \qquad (3)$$

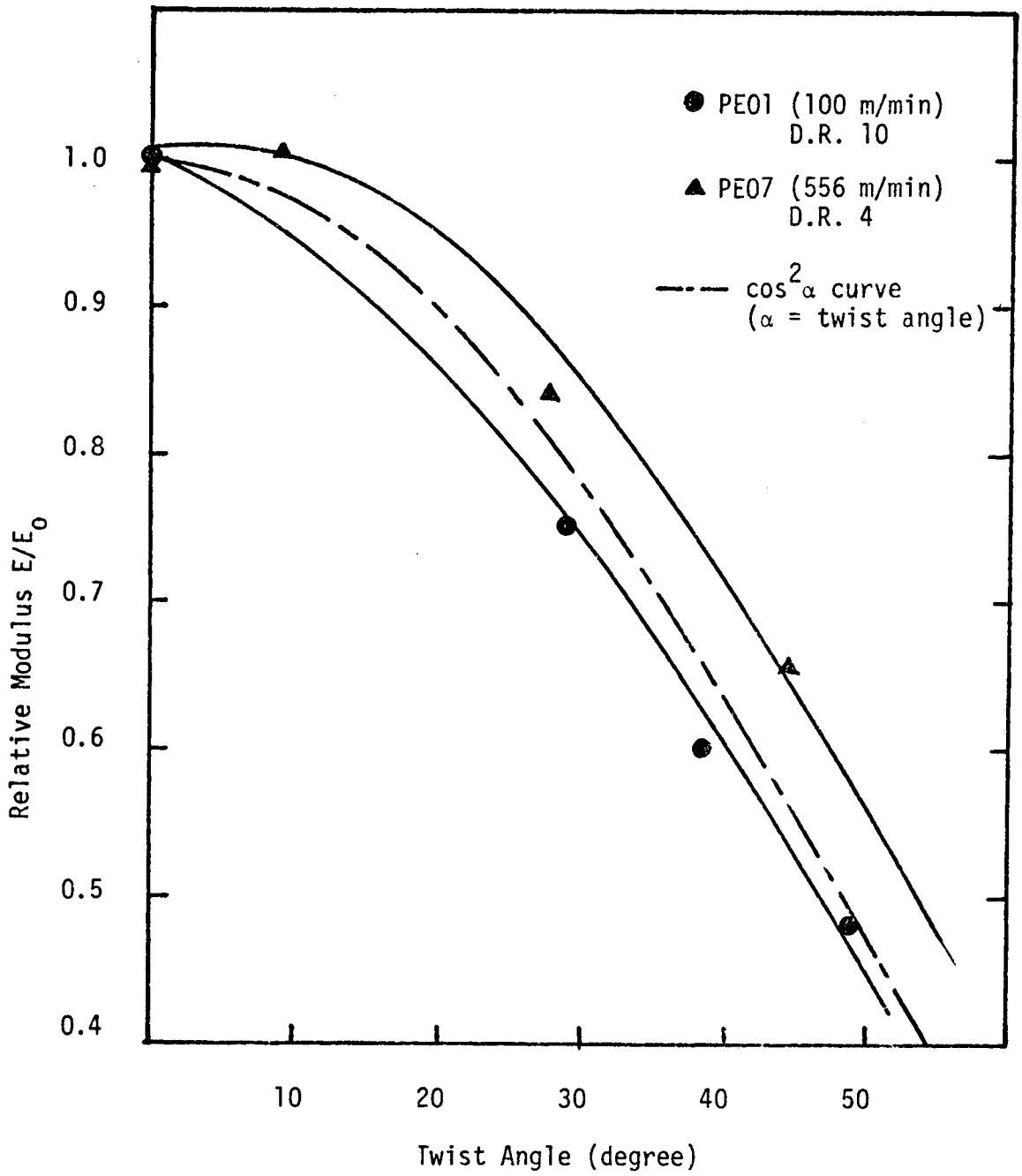


Figure 32. Effect of Twist Angle on Relative Modulus of Drawn HDPE Fibers (PE01 and PE07) at Room Temperature

where E_y is the tensile modulus of the yarn, E_f is the tensile modulus of the individual fibers, and α is the maximum twist angle. The derivation of Equation (3) presumes that the individual filaments obey Hooke's law and reflect lateral pressure effects which would influence filament tension. The fibers are assumed to be distributed across the yarn with the same twist factor (turns per unit length) which implies that the twist angle varies with radius from zero at the yarn axis to a maximum at its outer radius. According to the above analogy we might then expect

$$\frac{E \text{ (twisted fiber)}}{E \text{ (drawn fiber)}} = \cos^2\alpha \qquad (4)$$

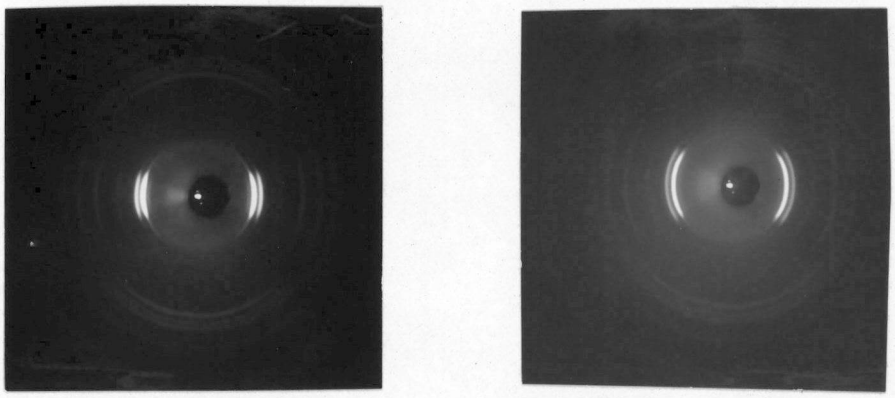
The fact that this equation is fairly well obeyed implies that it is reasonable to consider the fibrils in the twisted fiber to act independently of one another.

E. HEAT SETTING OF TWISTED FIBERS

X-Ray Studies

Figures 33 and 34 show the WAXS and SAXS patterns of the twisted fibers (PE01 and PE07) which have been heat set at 120°C for 30 minutes. It is noteworthy that the extra arc inside the (110) reflection disappears after heat setting (as shown in Figures 33 (a), 33 (c), 34 (a) and 34 (c)).

After annealing the SAXS patterns exhibit increased meridional and decreased equatorial scattering relative to that prior to annealing. The probable explanation for these changes is that the annealing allows



(a) (c)



(b) (d)

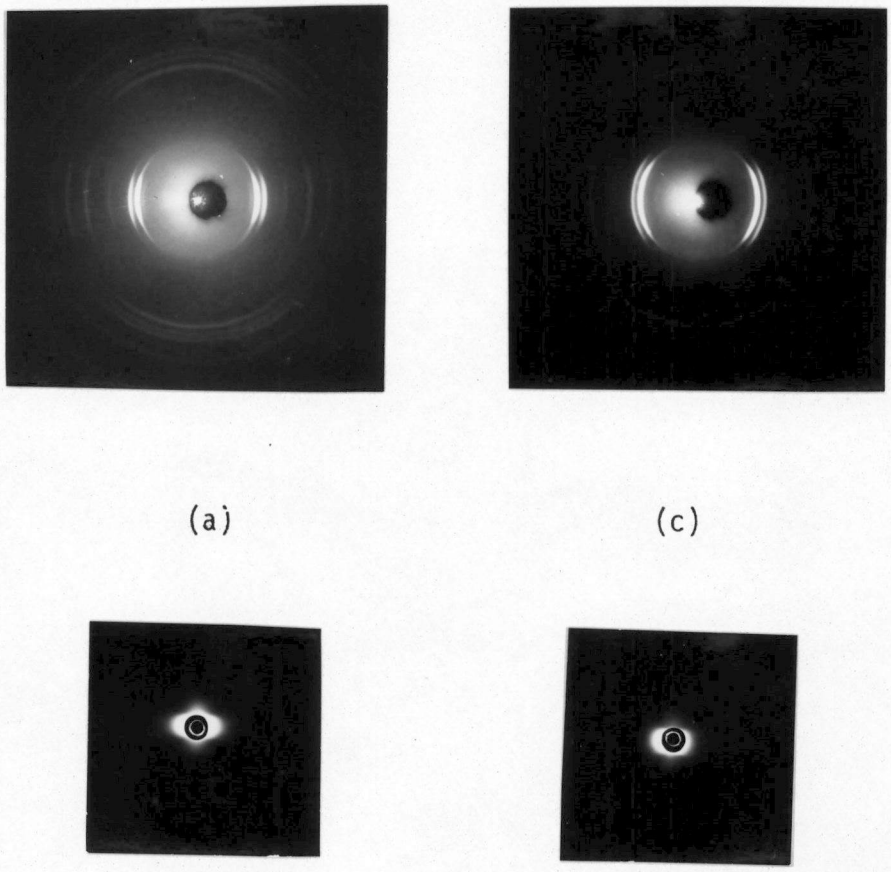
Figure 33. Diffraction Patterns of HDPE (PE01) Fibers (D.R. 10)

(a) WAXS twist 50 turns/inch, heat set at 120°C for 30 minutes

(b) SAXS twist 50 turns/inch, heat set at 120°C for 30 minutes

(c) WAXS twist 100 turns/inch, heat set at 120°C for 30 minutes

(d) SAXS twist 100 turns/inch, heat set at 120°C for 30 minutes



(a) (c)

(b) (d)

Figure 34. Diffraction Patterns of HDPE (PE07) Fibers (D.R. 4)

(a) WAXS twist 75 turns/inch, heat set at 120°C for 30 minutes

(b) SAXS twist 75 turns/inch, heat set at 120°C for 30 minutes

(c) WAXS twist 150 turns/inch, heat set at 120°C for 30 minutes

(d) SAXS twist 150 turns/inch, heat set at 120°C for 30 minutes

void healing and a consequent reduction in diffuse scattering together with some improvement in the perfection and regularity of chain folded crystals. The disappearance of the extra arc in the WAXS patterns after heat setting indicates that the strain induced phase transformation to the monoclinic form was reversed by annealing.

Scanning Electron Microscopy

In the case of twisted fibers which had been annealed, no obvious changes of surface texture could be observed and the results were similar to that shown in Figure 28, page 60.

Mechanical Properties

Figures 35 and 36 show the stress-strain curves for the drawn, twisted and heat set fibers. The modulus and the elongation to break decrease as the twist level increases in a fashion similar to that observed for the unannealed fibers, Figures 29 and 30, pages 43 and 46. Consequently, the relative moduli and relative breaking loads exhibit trends similar to the unannealed case, compare Figures 37 and 38 to Figures 31 and 32. Clearly, annealing at 120°C does not cause extensive changes in the mechanical behavior of the fiber. But one does note slight changes of the absolute values of the modulus, tensile strength and elongation to break due to the annealing at constant length. The changes in these quantities are tabulated in Table III and Table IV (see Appendix).

F. UNTWISTED FIBERS

X-Ray Studies

Figures 39 and 40 show the WAXS and SAXS patterns of twisted,

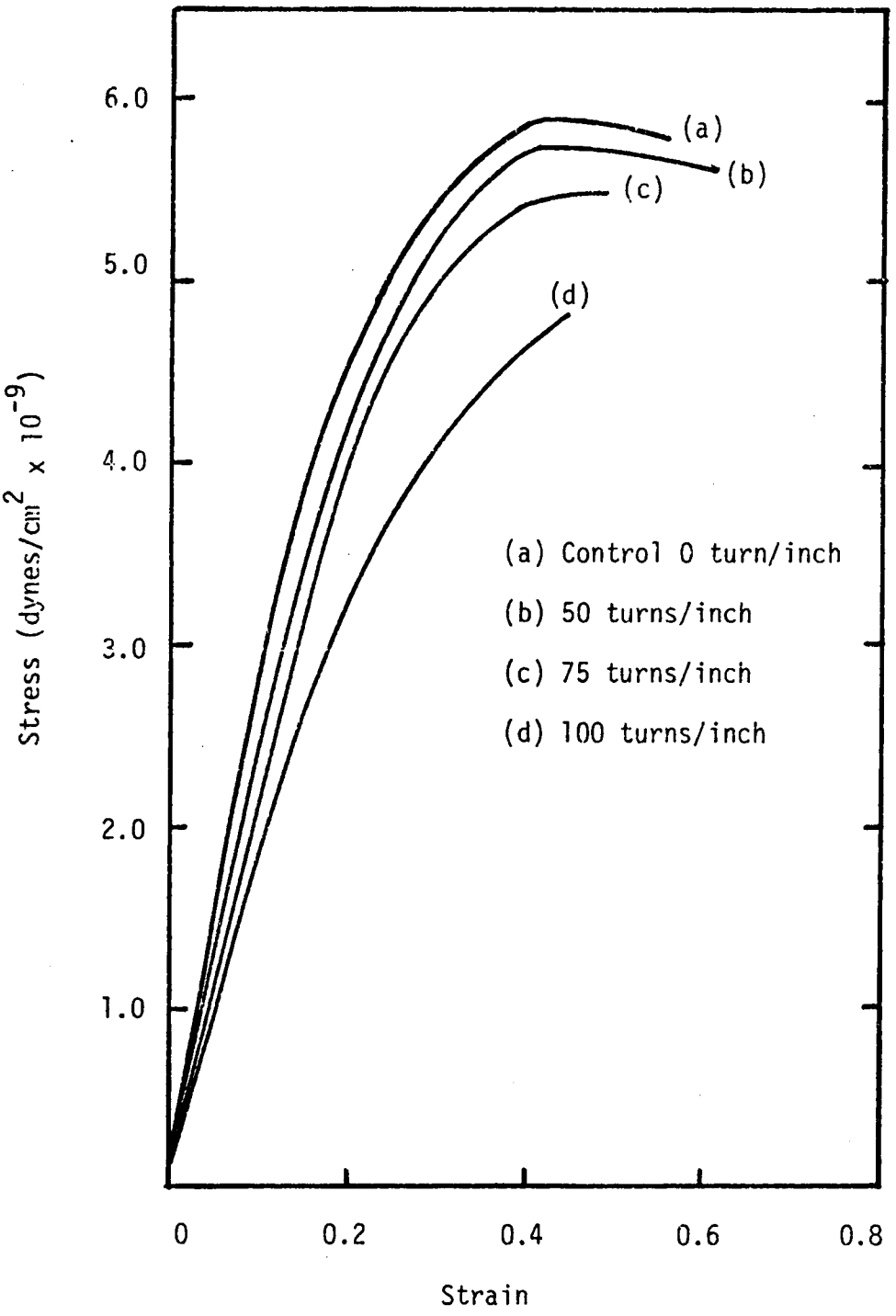


Figure 35. Stress Versus Strain Curve of Drawn PE01 (100 m/min) with Draw Ratio 10, Twist Various Amounts at Room Temperature, Heat Set at 120°C for 30 Minutes

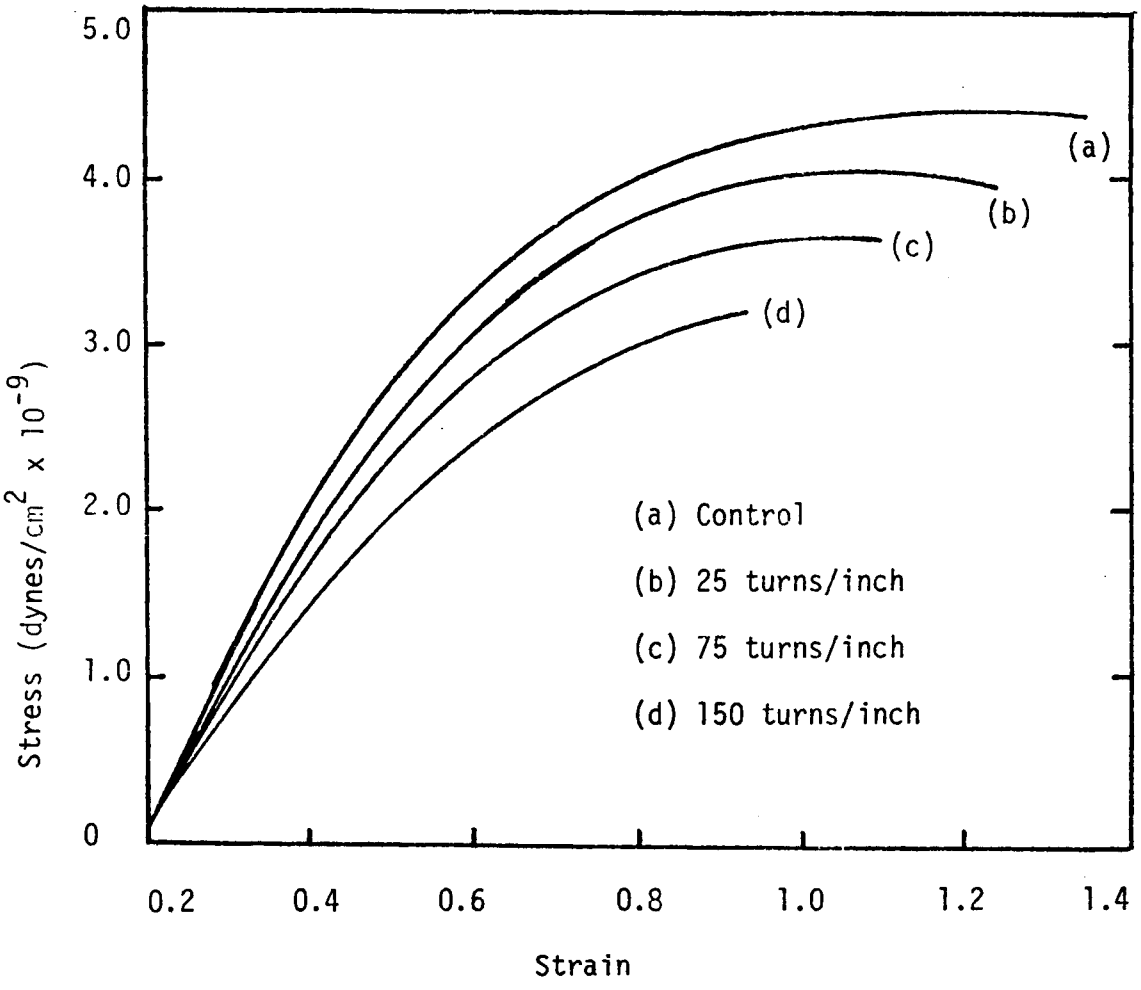


Figure 36. Stress Versus Strain Curve of Drawn PE07 (556 m/min) with Draw Ratio 4, Twist Various Amounts at Room Temperature, Heat Set at 120°C for 30 Minutes

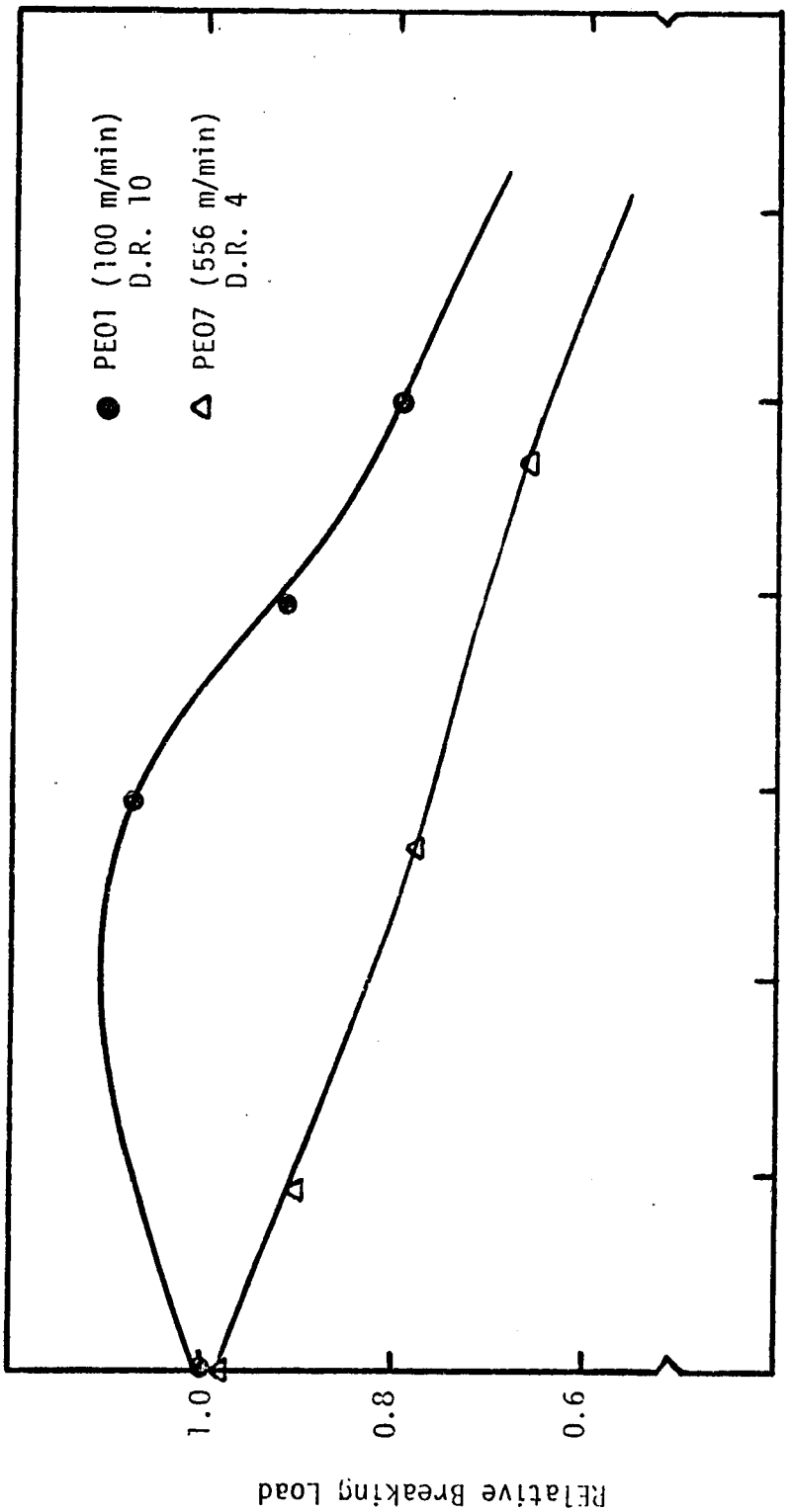


Figure 37. Effect of Twist Angle on Relative Breaking Load of Drawn HDPE Fibers (PE01 and PE07) at 120°C

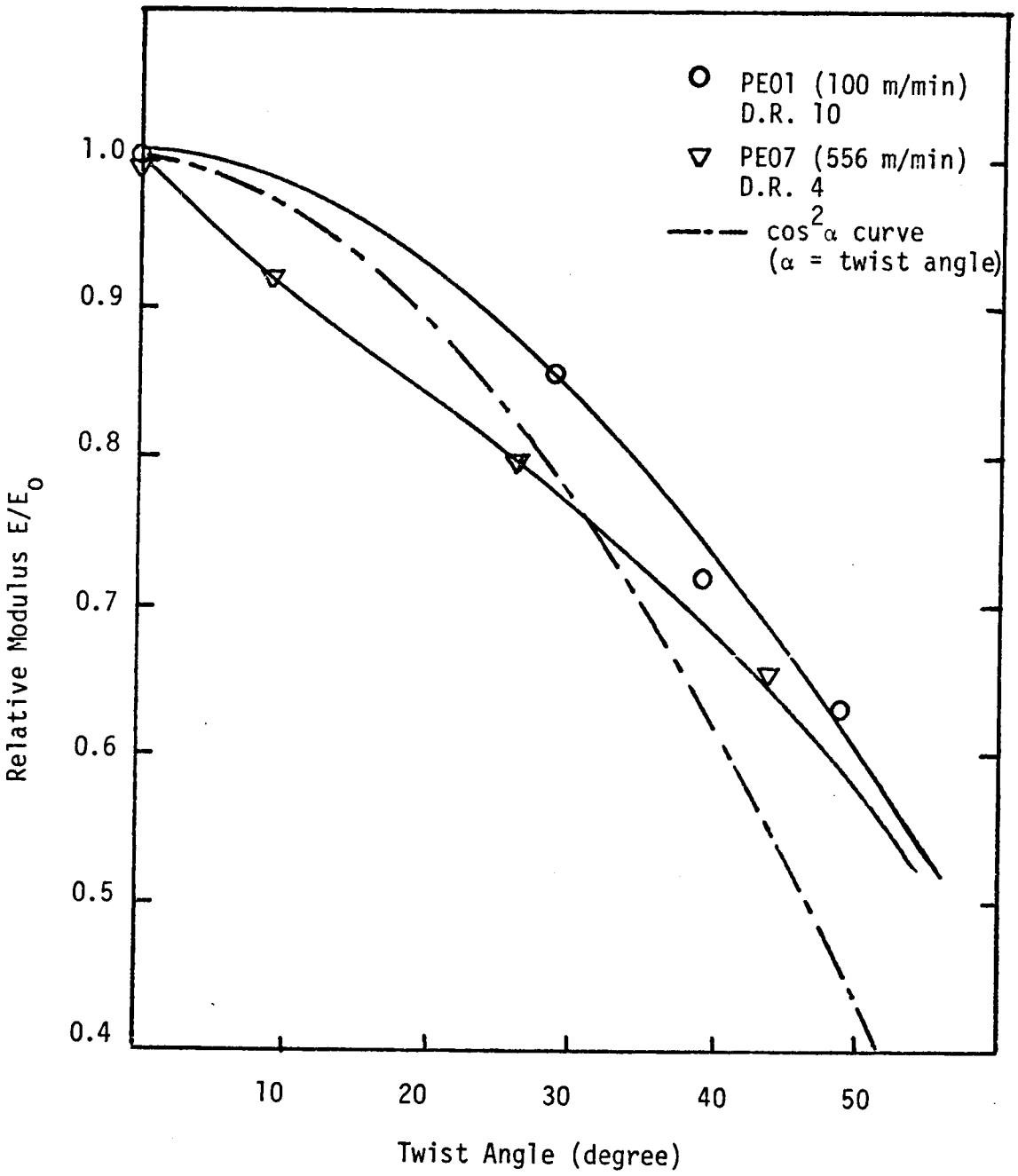
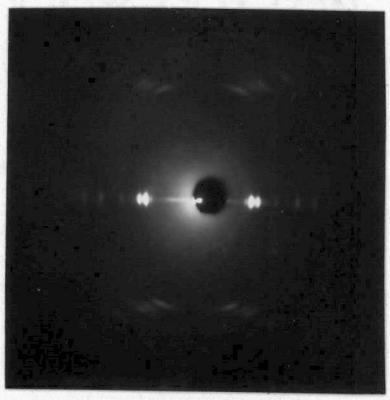
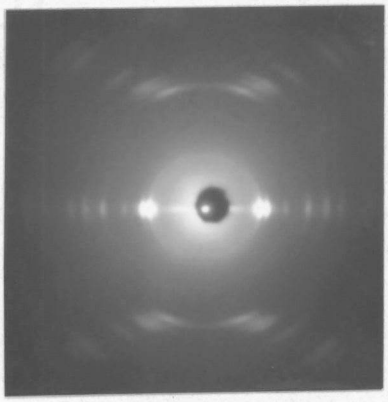


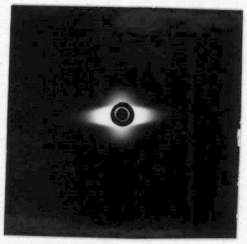
Figure 38. Effect of Twist Angle on Relative Modulus of Drawn HDPE Fibers (PE01 and PE07) at 120°C



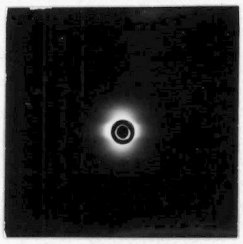
(a)



(c)



(b)



(d)

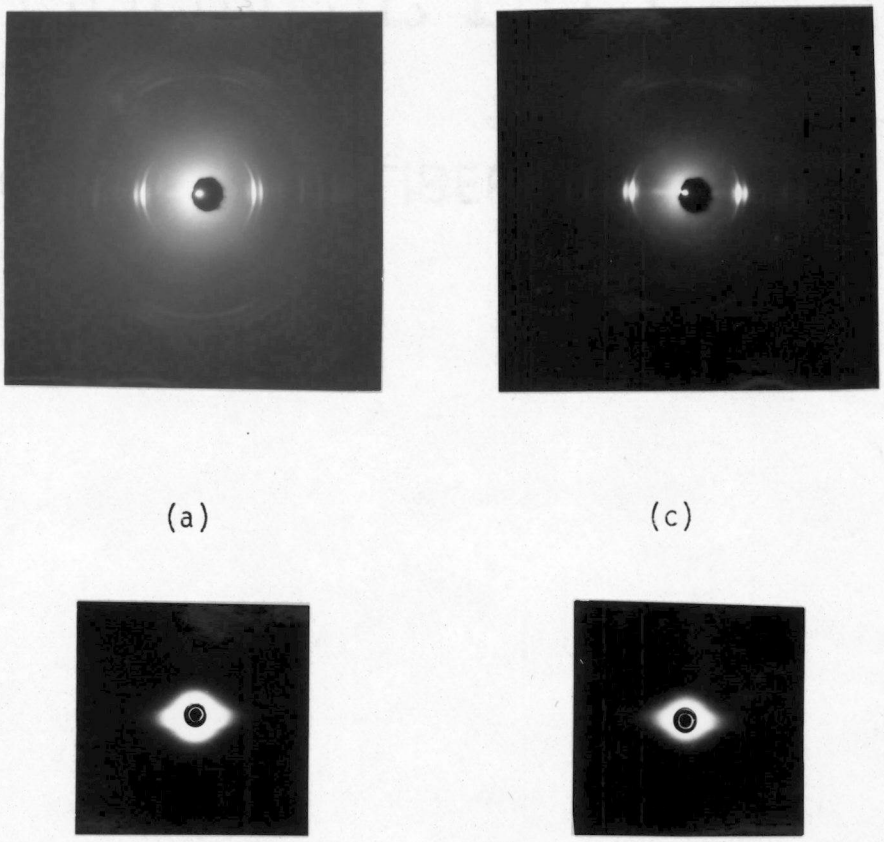
Figure 39. Diffraction Patterns of HDPE (PE01) D.R. 10

(a) WAXS twist 50 turns/inch, heat set at 120°C for 30 minutes, then untwisted

(b) SAXS twist 50 turns/inch, heat set at 120°C for 30 minutes, then untwisted

(c) WAXS twist 100 turns/inch, heat set at 120°C for 30 minutes, then untwisted

(d) SAXS twist 100 turns/inch, heat set at 120°C for 30 minutes, then untwisted



(a) (c)

(b) (d)

Figure 40. Diffraction Pattern of HDPE (PE07) D.R. 4

(a) WAXS twist 75 turns/inch, heat set at 120° for 30 minutes, then untwisted

(b) SAXS twist 75 turns/inch, heat set at 120°C for 30 minutes, then untwisted

(c) WAXS twist 150 turns/inch, heat set at 120°C for 30 minutes, then untwisted

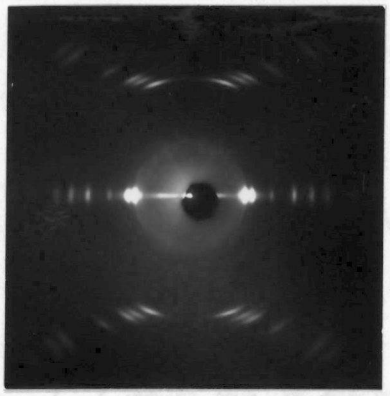
(d) SAXS twist 150 turns/inch, heat set at 120°C for 30 minutes, then untwisted

heat set and forcibly untwisted fibers. It is observed that the equatorial arcs of the WAXS patterns return back to spots similar to the original equatorial spots as if no twist had been imparted to the fibers. (Compare Figures 39 (a), 39 (c), 40 (a) and 40 (c) to Figures 19 (a) and 20 (a), pages 43 and 46.) An even better comparison is observed in Figure 41 where diffraction patterns of drawn and heat set samples (no twisting) are presented. Thus, the small differences observed between Figures 39 and 19 and between Figures 40 and 20 are due mainly to the heat setting and not the twisting and untwisting.

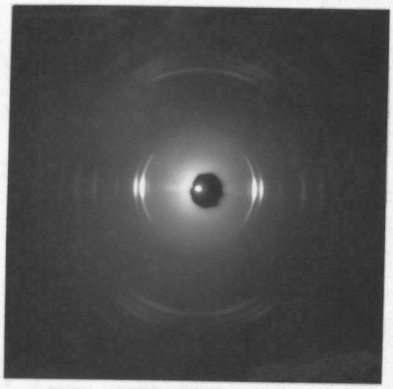
The SAXS patterns, Figures 39 (b), 39 (d), 40 (b), 40 (d), do not exhibit precisely the same features as they did prior to twisting and heat setting. The patterns for the annealed and untwisted fibers exhibit lower equatorial scattering and greater meridional scattering. However, annealing without twisting, Figure 41 (b) and 41 (d) causes similar changes in patterns for drawn fibers and it is believed that this is the main effect being observed. It is interesting that untwisting of the annealed fiber causes an increase in both the meridional and the equatorial scattering as compared to the annealed, twisted fiber. (Compare Figures 39 (b), 39 (d), 40 (b), 40 (d) to Figures 33 (b), 33 (d), 34 (b) and 34 (d).

Scanning Electron Microscopy

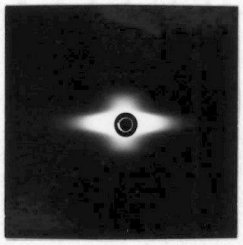
When the fibers are forcibly untwisted back to the initial state, the surface fibrils tend to tilt back to align themselves parallel to the fiber axis. The results from the SEM show that the process is not quite as simple as might be envisioned on the basis of the x-ray data



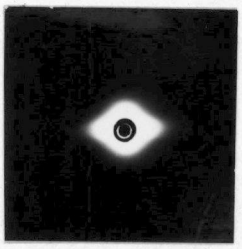
(a)



(c)



(b)



(d)

Figure 41. WAXS and SAXS Patterns of HDPE

(a) WAXS, PE01, D.R. 10, heat set at 120°C for 30 minutes

(b) SAXS, PE01, D.R. 10, heat set at 120°C for 30 minutes

(c) WAXS, PE07, D.R. 4, heat set at 120°C for 30 minutes

(d) SAXS, PE07, D.R. 4, heat set at 120°C for 30 minutes

alone. The surface of the fiber exhibits endless stacks of kink bands; that is, the surface fibrils make zig-zag paths (Figure 42). In order to see the kink bands more clearly, the untwisted fiber was etched in fuming nitric acid at 80°C for one hour. The result is shown in Figure 43.

One of the goals in this research was to establish the conditions for which kink bands form on the surface of the fibers. These were observed only for samples which were forcibly untwisted. Kinking occurred whether the fiber was heat set or not. Seto and Tajima (53) reported kink bands were formed in oriented polyethylene rods due the shear stress caused by compression loading. The present observation that kinking occurs only on untwisting suggests that it does not result from simple shear alone. In the present case it evidently requires the combination of two shears.

Mechanical Properties

The stress-strain curves of the untwisted fibers (PE01 and PE07) are shown in Figures 44 and 45. The tensile modulus of the untwisted fiber decreases compared with that of the control. The control is a drawn fiber which has been heat set at constant length but never twisted. Due to the constant length annealing and increased deformation of the fibers, the elongation to break is poor. Defects created by the twisting and untwisting cause premature fracture. One possible reason for the decrease in modulus is that the tie molecules between the fibrils in the deformed fiber may act less coherently in a tensile test as a result of the twisting and untwisting.



Figure 42. Scanning Electron Micrograph of PE01 with Draw Ratio of Ten, Twist at 100 Turns/Inch and Untwist

Double arrow indicates fiber axis.

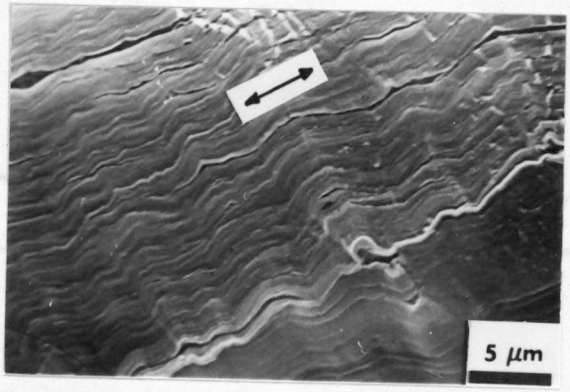


Figure 43. Scanning Electron Micrographs of PE03 (50 m/min) Etched in Fuming Nitric Acid for One Hour, D.R. 10, Twisted 125 Turns/Inch, Untwisted

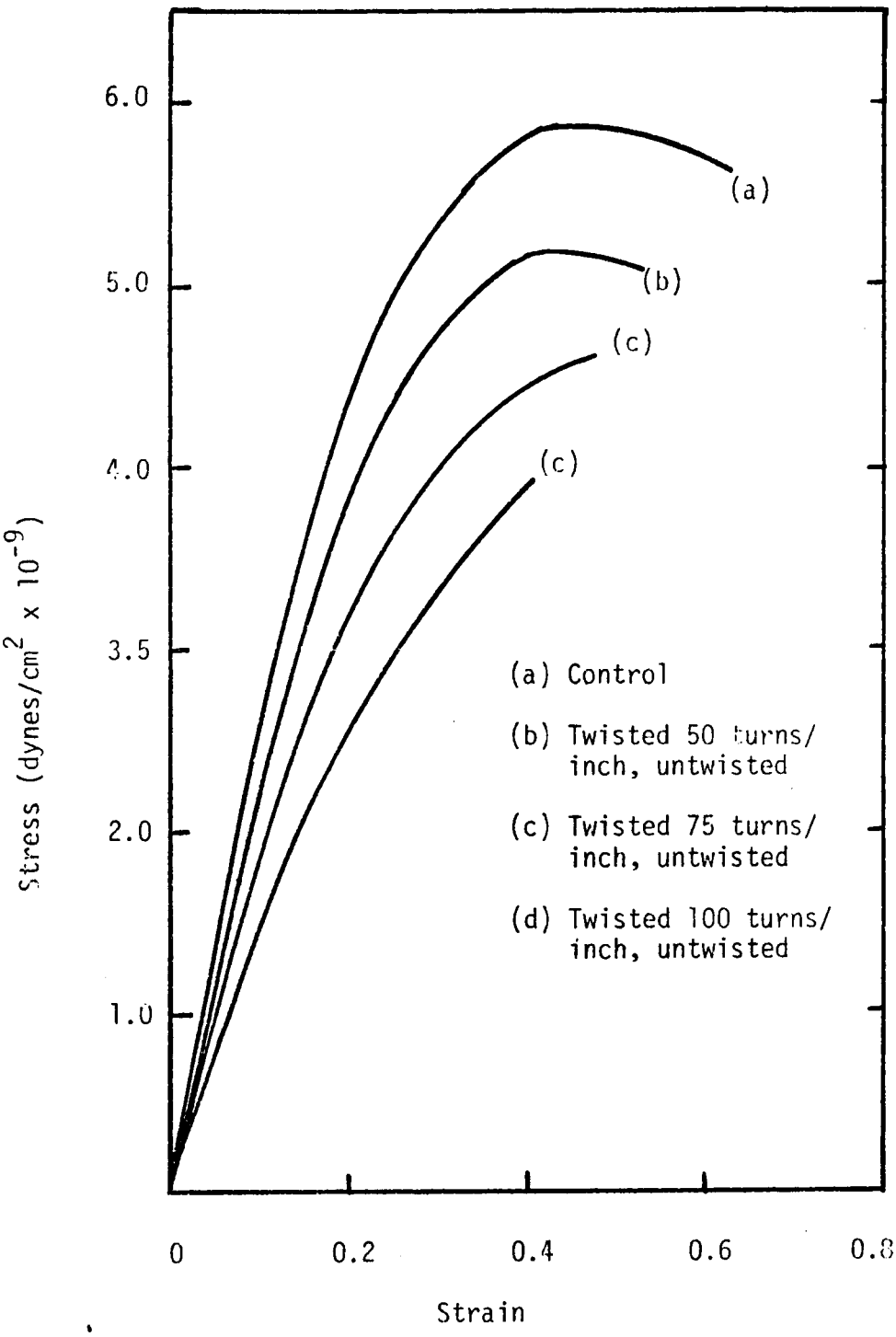


Figure 44. Stress Versus Strain Curve of Drawn PEO1 Fiber (100 m/min) with Draw Ratio 10, Twist at Various Amount, Heat Set at 120°C for 30 Minutes, Then Untwisted Back to Initial State

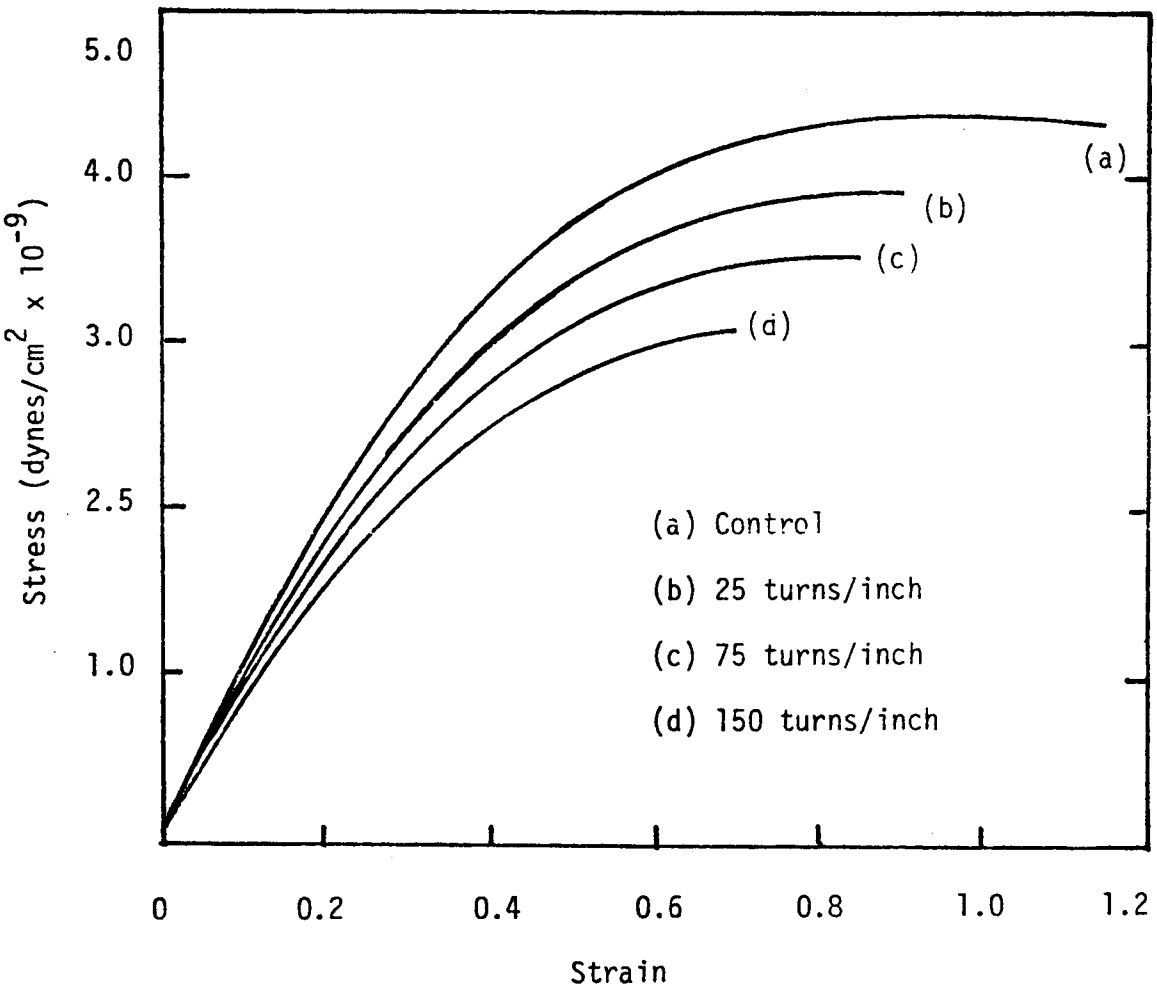


Figure 45. Stress Versus Strain Curve of Drawn PE07 Fiber (556 m/min) with Draw Ratio 4, Twist at Various Amounts at Room Temperature, Heat Set at 120°C for 30 Minutes, Untwisted Back to Initial State

CHAPTER V

CONCLUSIONS AND RECOMMENDATIONS

The major conclusions resulting from this study are briefly summarized below and are followed by recommendations for further study.

1. The behavior and response of melt spun polyethylene filaments during further processing operations such as drawing, twisting, heat setting and untwisting depends on the spinning conditions used in the production of the filaments. This was attributed to the difference in morphology developed by different spinning conditions.

2. Drawing at room temperature proceeds by necking. The tensile curve exhibits a yield point and extension to the "natural draw ratio" at nearly constant load. Both the natural draw ratio and the total elongation to break are greater for fibers spun at low stress, i.e., low take-up velocity, than at high stress.

3. Drawing results in a very high crystalline orientation in which the c-axes of the polyethylene crystals are essentially parallel to the fiber axis. Drawing also results in fibrillation and large increases in modulus and tensile strength. At a draw ratio slightly greater than the natural draw ratio, the amount of fibrillation decreases with increasing take-up velocity during spinning.

4. Twisting of either as-spun or drawn fibers decreased the axial orientation, modulus, tensile strength, and usually also the elongation to break. The change in these properties increased with increasing twist angle. Twisting also caused a transformation of a

small fraction of the sample to the monoclinic crystal structure.

5. For as-spun filaments twisting tended to remove the yield point and produce a more uniform elongation when the twisted fiber was loaded in tension.

6. A model suggested by yarn mechanics gave a reasonable prediction of the decrease in relative modulus and axial orientation due to twisting of drawn fibers.

7. Heat setting caused partial healing of elongated voids which were generated during drawing, increased the perfection and periodicity of the stacking of lamellar crystals, and caused the monoclinic polyethylene formed during twisting to transform back to the orthorhombic crystal modification. Heat setting also increased the modulus and tensile strength of the fibers.

8. Untwisting returned the orientation in the fiber to essentially that which it would have if it had not been twisted. However, scanning electron microscopy examination showed that the fibrils were not simply returned to their untwisted form, but that they contained numerous kink bands. The formation of kink bands presumably resulted from a compression of the fibrils along their axes during untwisting.

Recommendations for further study include using a densitometer scan of the WAXS fiber diagrams which would establish detailed intensity distributions of the different reflections. This would help to better characterize the state of crystal orientation in the twisted fibers.

The present type of study should be extended to include other polymers including some of greater commercial interest such as

nylon 6, nylon 66, and polyethylene terephthalate. In addition, the experimental capabilities should be extended to the development of equipment for continuous drawing, twisting, draw-twisting and false-twist texturing.

LIST OF REFERENCES

LIST OF REFERENCES

1. Abbott, L. E. and J. L. White, Appl. Poly. Symp., 20, 247 (1973).

2. Acierno, D., J. N. Dalton, J. M. Rodriguez and J. L. White, J. Appl. Poly. Sci., 15, 2395 (1971).

3. Andrichenko, Y. D., T. V. Duizhinina, Y. A. Zubov, A. A. Koukin and D. Y. Tsvaikin, Vysokomol Soyed, 7, 2126 (1965).

4. Arthur, D. F., J. Text. Inst., 49, 638 (1958).

5. Barrwens, J. C., C. Barrwens-Crowet and G. Homes, J. Poly. Sci., 7, 1745 (1969).

6. Bettlehein, F. A. and R. S. Stein, J. Poly. Sci., 31, 523 (1958).

7. Billmeyer, F. W., Jr. Textbook of Poly. Sci., Interscience, New York (1962).

8. Carothers, W. H. and J. W. Hill, J. Amer. Chem. Soc., 54 (1974).

9. Chen, J. J., G. E. Hagler, L. E. Abbott, D. C. Bogue and J. L. White, Trans. Soc. Rheology, 16, 473 (1972).

10. Cooper, S. L., A. J. McKinnon and D. C. Prevorsek, Text. Res. J., 38, 803 (1968).

11. Cooper, S. L., A. J. McKinnon and D. C. Prevorsek, J. Poly Sci., (A-1) 6, 353 (1968).

12. Dees, J. R. and J. E. Spruiell, J. Appl. Poly. Sci., 18, 1053 (1974).

13. Dees, J. R., Ph.D. Dissertation, Department of Chemical and Metallurgical Engineering, The University of Tennessee, Knoxville, Tennessee, 1974.

14. Dent, R. W. and J. W. S. Hearle, Text. Res. J., 30, 505 (1960).

15. Fankuchen, I. and H. Mark, J. Appl. Phys., 15, 368 (1944).

16. Fisher, E. W., Z. Nature Fosch., 12a, 753 (1957).

17. Fisher, E. W. and K. Bacon, Eds. New Methods of Polymer Characterization, Interscience, New York (1964). P. 316.

18. Frank, F. C., A. Keller and A. O'Connor, Phil. Mag., 3, 64 (1958).

19. Gegauff, G., Bull. Soc. Ind. Mulhouse, 77, 153 (1907).

20. Geil, P. H. Poly. Single Crystals, Interscience Publishers, New York, 1963. Chapter 5.

21. Glanz, W., A. Peterlin and W. Wilkes, J. Poly. Sci., pt. A-2, 9, 1243 (1971).

22. Happy, F., H. S. Peiser, H. P. Kookstory and A. J. C. Wilson, Eds., X-Ray Diffraction by Polycrystalline Materials, Chapman and Hall, London (1962).

23. Hearle, J. W. S., J. T. Sparrow and P. M. Cross. The Use of the Scanning Electron Microscope, Pergamon Press, 1972.

24. Hearle, J. W. S., J. Text. Inst., Trans., 49, T389 (1958).

25. Hein, N. V., S. L. Cooper and J. A. Koutsky, J. Macromol. Sci., B6, 343 (1972).

26. Herman, K. O. Gergross and W. Abitz, Z. Physik Chem., B10, 371 (1930).

27. Hess, K., J. Colloid Sci., Suppl. 1, 135 (1954).

28. Hosemann, R., Acta. Cryst., 4, 520 (1951).

29. Keller, A., Phil. Mag, 2, 1171 (1957).

30. Kiho, H., A. Peterlin and P. H. Geil, J. Appl. Phys., 35, 1599 (1964).

31. Lazurkin, J. S., J. Poly. Sci., 30, 595 (1958).

32. Mark, H. and K. H. Meyer, Z. Physik. Chem., B2, 115 (1929).

33. Marshall, I. and A. B. Thompson, Proc. Roy Soc. (London), A221, 541 (1954).

34. Matsuokas, "Dilatometric Observation of Annealing Process in Bulk Polyethylene," paper presented at Am. Phys. Soc. Meeting, Baltimore, Maryland, 1962.

35. Meinel, G. and A. Peterlin, J. Poly. Sci., A-2, 9, 67 (1967).

36. Muzzy, J. P. and D. Hansen, Text. Res. J., 41, 436 (1971).

37. O'Leary, K. and P. Geil, J. Appl. Phys., 38, 4169 (1967).

38. Padden, P. J. and H. D. Keith, J. Appl. Phys., 30, 1479 (1959).

39. Peterlin, A. and E. Roeckl, J. Appl Phys., 34, 102 (1963).

40. Peterlin, A. and F. Balta-Calleja, J. Appl. Phys., 40, 4238 (1968).

41. Peterlin, A. and G. Meinel, Makromolekulare Chemie, 142, 227 (1971).

42. Prevorsek, D. C. and W. J. Lyons, Text. Res. J., 35, 581 (1965).

43. Robertson, R. E., J. Appl. Poly. Sci., 7, 443 (1963).

44. Robertson, R. E., J. Poly. Sci., A-2, 1315 (1969).

45. Robertson, R. E., J. Poly. Sci., A-2, 9, 453 (1971).

46. Robertson, R. E., J. Poly. Sci., A-2, 9, 1255 (1971).

47. Sakaoku, K and A. Peterlin, J. Poly. Sci., A-2, 9, 895 (1971).

48. Samuels, R., ACS Polymer Preprints, 10, 1218 (1969).

49. Samuels, R., J. Macromol. Sci. Phys., B4, 701 (1970).

50. Samuels, R. J., J. Poly. Sci., pt. A-2, 6, 2021 (1969).

51. Scott, R. G., Symposium on Microscopy, ATSM Special Technical Publication No. 257, p. 121 (1959).

52. Seto, T. and Y. Tajima, Jap. J. Appl. Phys., 5, 523 (1966).

53. Seto, T., T. Hara and K. Tanaka, Jap. J. Appl. Phys., 7, 31 (1968).

54. Sikorski, J., J. S. Moss, P. H. Newman and T. Buckley, J. Sci. Inst., Series 2, I, 29 (1968).

55. Slichter, W. P., J. Poly. Sci., V-21, 112 (1956).

56. Statton, W. O., J. Poly. Sci., 58, 205 (1962).

57. Statton, W. O., J. Poly. Sci., C-18, 33 (1967).

58. Staudinger, H. Die Hochmolekularan Organischen Verbindungen, Springer-Verlag, Berlin, 1932.

59. Stein, R. S. and F. H. Norris, J. Poly. Sci., 21, 381 (1956).

60. Till, P. H., J. Poly. Sci., 24, 301 (1957).

61. White, J. L., K. C. Dharod and E. S. Clark, J. Appl. Poly. Sci., V-18, 2539 (1974).

62. Wilkinson, Texturized Yarn Technology, Volume 1, Monsanto, 1967.

63. Williams, J. and A. Peterlin, J. Poly. Sci., A-2, 9, 1483 (1971).

64. Wilson, O., Ind. Eng. Chem., 18, 829 (1926).

65. Zaukelies, D. A., J. Appl. Phys., 33, 2797 (1962).

APPENDIX

TABLE I

SPINNING CONDITIONS FOR THE FIBER STUDIED IN DEPTH

NAME	PE01	PE07
Extrusion Rate g/min	1.930	1.911
Melt Temperature (°C)	205	210
Take-up Velocity (m/min)	100	556
Spinning Stress dynes/$cm^2 x 10^{-6}$	2.80	17.1
Ambient Temperature (°C)	28.0	28.5
Diameter (cm)	0.01793	0.00833

TABLE II

COMPARISON BETWEEN THE MAXIMUM TILT ANGLE OBTAINED FROM THE X-RAY PATTERN WITH THAT DIRECTLY MEASURED FROM THE SURFACE OF TWISTED FIBER IN THE SCANNING ELECTRON MICROGRAPH

	PE01			PE07		
Name	50 turns/in	75 turns/in	100 turns/in	25 turns/in	75 turns/in	150 turns/in
X-Ray	20°	30°	35°	6°	12°	30°
Scanning Micrograph	22°	31°	42°	7°	15°	38°

TABLE III

COMPARISON OF THE CHANGES OF THE MODULUS, ELONGATION TO BREAK, AND TENSILE STRENGTH OF PEO1 AT ROOM TEMPERATURE AND AT 120°C

	Room Temperature			Heat Set at 120°C for 30 Min		
PEO1	Modulus dynes/cm^{2}x10^{-9}	Elongation to Break (%)	Tensile Strength dynes/cm^{2}x10^{-9}	Modulus dynes/cm^{2}x10^{-9}	Elongation to Break (%)	Tensile Strength dynes/cm^{2}x10^{-9}
0 turns/in	22.22	75	4.81	23.52	56	5.85
50 turns/in	20.41	84	4.61	21.27	61	5.72
75 turns/in	14.28	71	4.42	19.67	49	5.49
100 turns/in	11.11	65	4.15	12.50	44	4.78

TABLE IV

COMPARISON OF THE CHANGES OF THE MODULUS, ELONGATION TO BREAK AND TENSILE STRENGTH OF PE07 AT ROOM TEMPERATURE AND AT 120°C

	Room Temperature			At 120°		
PE07	Modulus dynes/cm^2x10^{-9}	Elongation to Break (%)	Tensile Strength dynes/cm^2x10^{-9}	Modulus dynes/cm^2x10^{-9}	Elongation to Break (%)	Tensile Strength dynes/cm^2x10^{-9}
0 turns/in	7.69	122	3.45	9.09	115	4.41
25 turns/in	8.10	104	3.55	8.33	103	4.03
75 turns/in	6.45	76	3.35	7.14	89	3.65
150 turns/in	5.12	78	2.91	5.88	74	3.31

VITA

Gordon Ming Sze was born in Shangai, China, on December 8, 1948. He went to Hong Kong in 1959, where he attended high school and received the Secondary School Certificate in 1967. In September 1967, he came to the United States and entered the Northwestern State University in Louisiana. Two years later, he transferred to the University of Texas at Austin and received the Bachelor of Science degree in Chemical Engineering in May 1972.

Upon graduation he entered the Graduate School at The University of Tennessee and received the Master of Science degree with a major in Chemical Engineering in March 1975.